Response to Reviewer #1

Overview: *This manuscript describes a novel approach to SERS analysis of aerosol particles, where the nanoparticles are deposited onto the aerosol surface, as opposed to aerosol particles being deposited onto a more conventional SERS substrate. The manuscript thoroughly considers the prior Raman and SERS literature and makes a significant step forward in the spectroscopic analysis of aerosol particles. There are some significant shortcomings that need to be addressed, but overall this is manuscript has many positive features.*

Response: The authors like to thank the reviewer for the valuable comments. We have added more information in the revised manuscript based on the reviewer's comments. Revised and added text in the main manuscript and supporting information was highlighted in red.

Major comments

Comment #1: SERS is often most enhanced when two metal nanoparticles are at specified distance from each other with a predetermined geometry. How ordered are these nanoparticles? What methods have been used to image the silver nanoparticles are the aerosol particle surface? Is the assumption that the enhancement is coming entirely from individual silver nanoparticles?

Response: (1) We expect that most Ag nanoparticles are individually deposited on the particle surface without much aggregation. Ag nanoparticles used in the current study were synthesized by the citrate-reduction method. If the nanoparticles were aggregated, SERS spectrum would show enhanced peaks of citrate adsorbed on Ag nanoparticle surface as stabilizer (Munro et al., 1995). In our measurements of AS particles, we observed strong citrate peaks only for one analyte particle (Fig. S1(e), see comment #5), but absent for all other SERS spectra. This gives us confidence that the enhancement is mainly coming from individual Ag nanoparticles. To address the above consideration, we have added the following text (lines 287-292):

"Ag nanoparticles used in the current study were synthesized by the citrate-reduction method. If the nanoparticles were aggregated, SERS spectrum would show enhanced peaks of citrate adsorbed on Ag nanoparticle surface as stabilizer (Munro et al., 1995). In our measurements of AS particles, we observed strong citrate peaks only for one particle (Figure S1(e)), but absent for all other SERS spectra. This gives us confidence that the enhancement is mainly coming from individual Ag nanoparticles."

(2) We have attempted to use SEM to visualize the presence of Ag nanoparticles on AS particles. However, the electron beam of SEM caused sample damage, leading to morphological changes to AS particle surface (see SEM images of a and b in Fig. A), in the absence of Ag nanoparticles. Moreover, the non-conductive AS particles were significantly charged so that the SEM image was distorted. The magnified image of AS particle (Fig. A (c)) shows protrusions that resemble Ag nanoparticles, but it is difficult to distinguish the nanoparticles from protrusions due to the morphological changes of AS. We have also attempted EDX analysis (JSM-6390, JEOL) but no signal of Ag element was observed probably because of the low concentration of Ag nanoparticles (Fig. B).
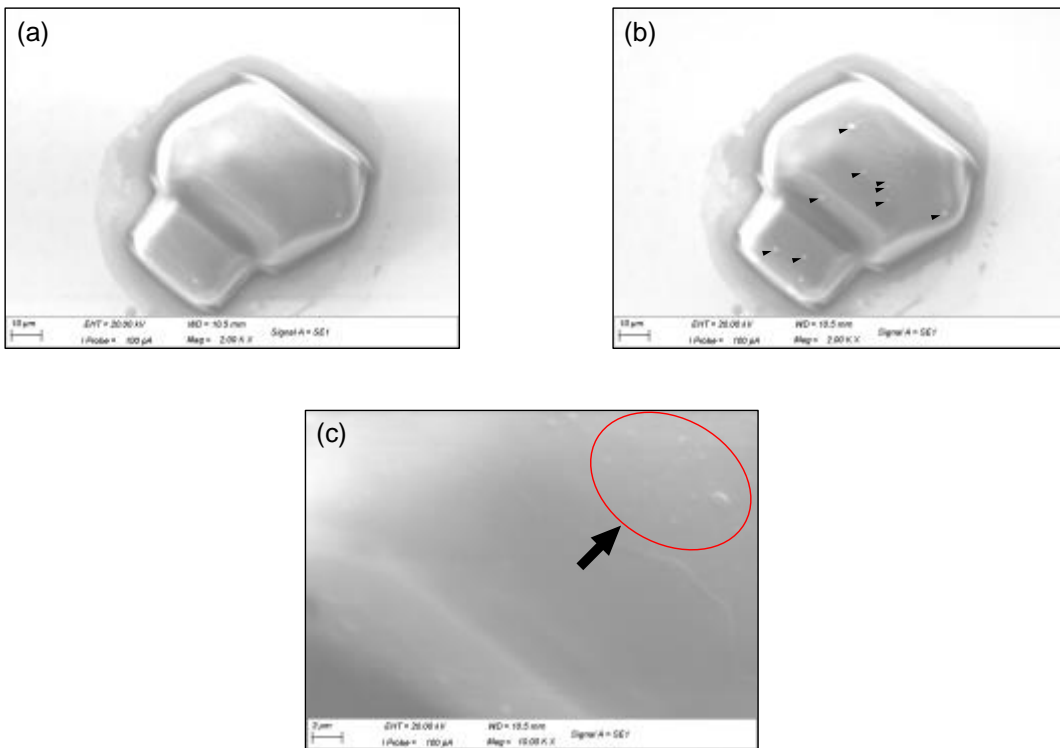
Figure A. SEM images of AS particle before (a) and after (b) an electron beam damage during observation. (c) an enlarged view of the surface of AS particle.
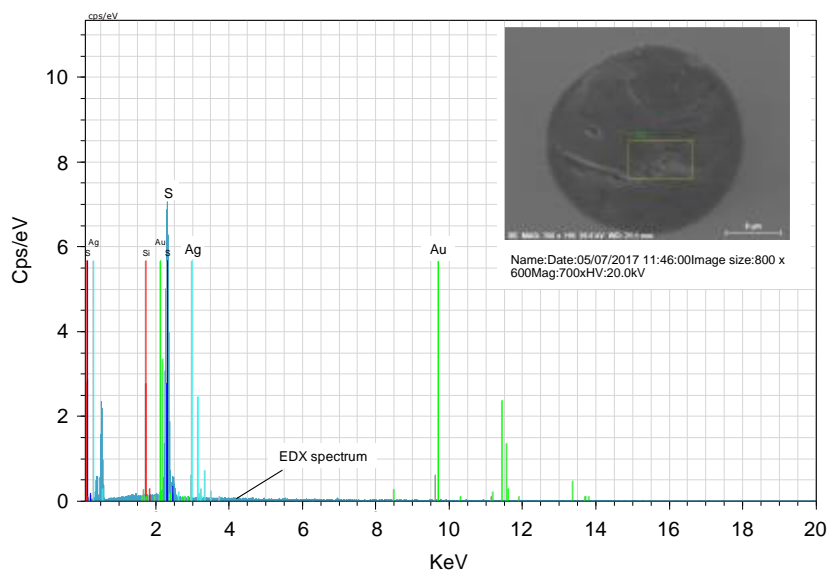
Figure B. EDX analysis of AS particle with Ag nanoparticle. The spectrum shows the peak of element of sulfur (i.e. SO_4) at ~2.3 KeV. No other elements were observed.

Comment #2: The size of the particles used calls some of the relevance of the findings into question. For example in Figure 3 the particles are 23 and 47 microns. It would be very helpful to have Raman of AS particles on top of silver nanoparticles for comparison. At these sizes it would not be surprising to see nanoparticles on top making a difference versus nanoparticles underneath, but no data on is given to support this claim. Also an optical image in the main text of AgNPs on top of the AS particles would be helpful are for particles 10s of microns in size, should be relatively easy to image.

Response: (1) The current manuscript is a proof-of-concept study for application of ES-SERS in chemical analysis of atmospherically relevant particles. As mentioned in the section 3.3, enhanced peaks at ~970 cm^{-1} did not drop as the size of analyte particle was down to 1.4 µm. This result demonstrates that the ES-SERS has the potential to characterize particles with atmospherically relevant size (below 1 µm). The above discussion has been described in the third paragraph in the conclusion.

(2) It is apparent that enhanced spectra from two cases (1) ES-SERS (Ag nanoparticles on the top of analyte particles) and (2) conventional SERS substrate (the nanoparticles underneath analyte particles) come from the different positions of analyte particles. SERS is a type of surface spectroscopy, which means that only the analyte molecules adsorbed to Ag nanoparticles contribute to the enhancement and its effect is the distance dependence (Dieringer et al., 2006). Therefore, ES-SERS is more sensitive to the surface of the analyte particles and is useful for surface characterization of atmospheric particles.

Although we do not have the data of direct comparison between the ES-SERS and conventional SERS substrates, we have compared our results with earlier works in the literature. We have added the following text and revised the corresponding text accordingly (lines 389-397):

"Craig et al. (2015) reported an enhancement factor of 2.0 at $\nu(SO_4^{2-})$ mode of ~970 cm^{-1} using an SERS substrate with the AS particles on the top of Ag nanoparticles on the substrate. Furthermore, Fu et al. (2017) reported an enhancement factor of 6.1 for the same mode, using commercial SERS substrates with pre-determined gold-coated structure of inverted pyramids (Klarite, Renishaw Diagnostics Ltd.). Our results of AS/sucrose particles (Table 1) showed that the I_{SERS}/I_{NR}, which is the lower limit of enhancement factor, ranged from 12.4 to 163, much higher than the above studies. Note that I_{SERS}/I_{NR} is the lower limit of the enhancement factor ($I_{SERS}N_{vol}/I_{NR}N_{surf}$) conventionally used because N_{vol}/N_{Surf} is much greater than unity in the present case."

(3) The optical images of AS particles with and without Ag nanoparticles have been shown in Fig. S6.

Comment #3: Calculation of enhancement factors? Relative enhancement of specific modes?

Response: As mentioned in the section 2.4, we did not calculate enhancement factors because the estimation of the number of analyte molecules adsorbed onto Ag nanoparticles is rather difficult. Instead, we compared enhanced intensity with normal Raman intensity as defined as I_{SERS}/I_{NR} based on earlier works (Fu et al., 2017; Le Ru et al., 2007). The I_{SERS}/I_{NR} gives information on relative enhancement of each vibration mode as summarized in Table 1. The relative enhancement was clearly observed at $\nu(SO_4^{2-})$ mode for the AS/sucrose particles (Fig. 3). The I_{SERS}/I_{NR} at $\nu(SO_4^{2-})$ mode is approximately 7.6 times higher than that at ν(C-H) mode (Table 1). This is likely due to the strong interaction between aqueous sulfate and Ag nanoparticles. To highlight this, we have added the following text (lines 274-276):

"The I_{SERS}/I_{NR} at $\nu(SO_4^{2-})$ mode is approximately 7.6 times higher than that at ν(C-H) mode (Table 1). This is likely due to the strong interaction between sulfate and Ag nanoparticles."

Comment #4: Optical and electron microscopy imaging of particles with and without nanoparticles on top would strongly improve the authors claims that the particles are sitting on top.

Response: Optical images of particles with and without Ag nanoparticles have been shown in Fig. 6 in the revised main manuscript. As mentioned in the response to comment #1, electron microscopy imaging was not useful to visualize Ag nanoparticles on AS particles. We believe that Ag nanoparticles are deposited on analyte particles because (i) enhanced peaks were observed only when the electrospraying was performed and (ii) the electrospray system enables deposition of Ag nanoparticles on any surface (from metallic to non-metallic substrate). In the comparison of the normal Raman and SERS spectra as shown in Fig 3, it is apparent that there is significant signal enhancement in SERS. Since the deposition of Ag particles was the only procedural difference in the two types of samples, we cannot think of any other possibilities that would lead to the enhancement. Hence we are confident that the ES-SERS can enhance the Raman signals. The latter point has been discussed in earlier work in the electrospray system (Gen and Lenggoro, 2015) that electrostatic deposition is dominant, compared to other mechanisms such as Brownian diffusion and gravitation. Therefore, Ag nanoparticles under the given electric fields can be deposited on a substrate as well as on AS particles. To address the reviewer's comment, we have added the following text (lines 284-287):

"The electrospray system has been proven to be effective in depositing nanoparticles onto any surface (Gen and Lenggoro, 2015). We believe that Ag nanoparticles are deposited onto the analyte particle surfaces because Raman enhancement was observed only when electrospraying Ag nanoparticles was performed."

Comment #5: Only a few particles are analyzed throughout the entire paper. Some details on the reproducibility, consistency of enhancements, and overall quantification are needed to truly show that this is a method that can be extrapolated to other aerosol studies. As of right now with so few spectra there could be concerns that only the best examples were chosen, which more statistics would help alleviate.

Response: We have investigated 22 laboratory particles in total (AS, AS/SA and AS/sucrose particles). We have showed the results of two AS (Fig. 4), two AS/SA (Fig. 4) and nine AS/sucrose particles (Figs. 3, 5 and 6) in the original main manuscript with and without Ag nanoparticles. Furthermore, more than 10 spectra were obtained for each particle by scanning the surface from one edge to another edge to quantify the intensity ratio of I_{SERS}/I_{NR}. Therefore, more than 220 spectra were taken into consideration for overall quantification of I_{SERS}/I_{NR} in Table 1. To address the reviewer's comments, we have added all spectra used (except for AS/sucrose particles smaller than 20 µm) for overall quantification of I_{SERS}/I_{NR} in the revised supporting information as Figs. S1, S2 and S3, and the following text in the revised manuscript to reflect this (lines 231-233). As shown in Figs. S2 and S3 (d) and (e), Raman enhancements at $v(SO_4^{2-})$ and $\delta(OH\cdots O)$ (only for AS/SA particles), and v(C-H) modes are observed for most spectra.

"All spectra for quantification of I_{SERS}/I_{NR} (except for AS /sucrose particles smaller than 20 µm) are shown in Figs. S1, S2 and S3."
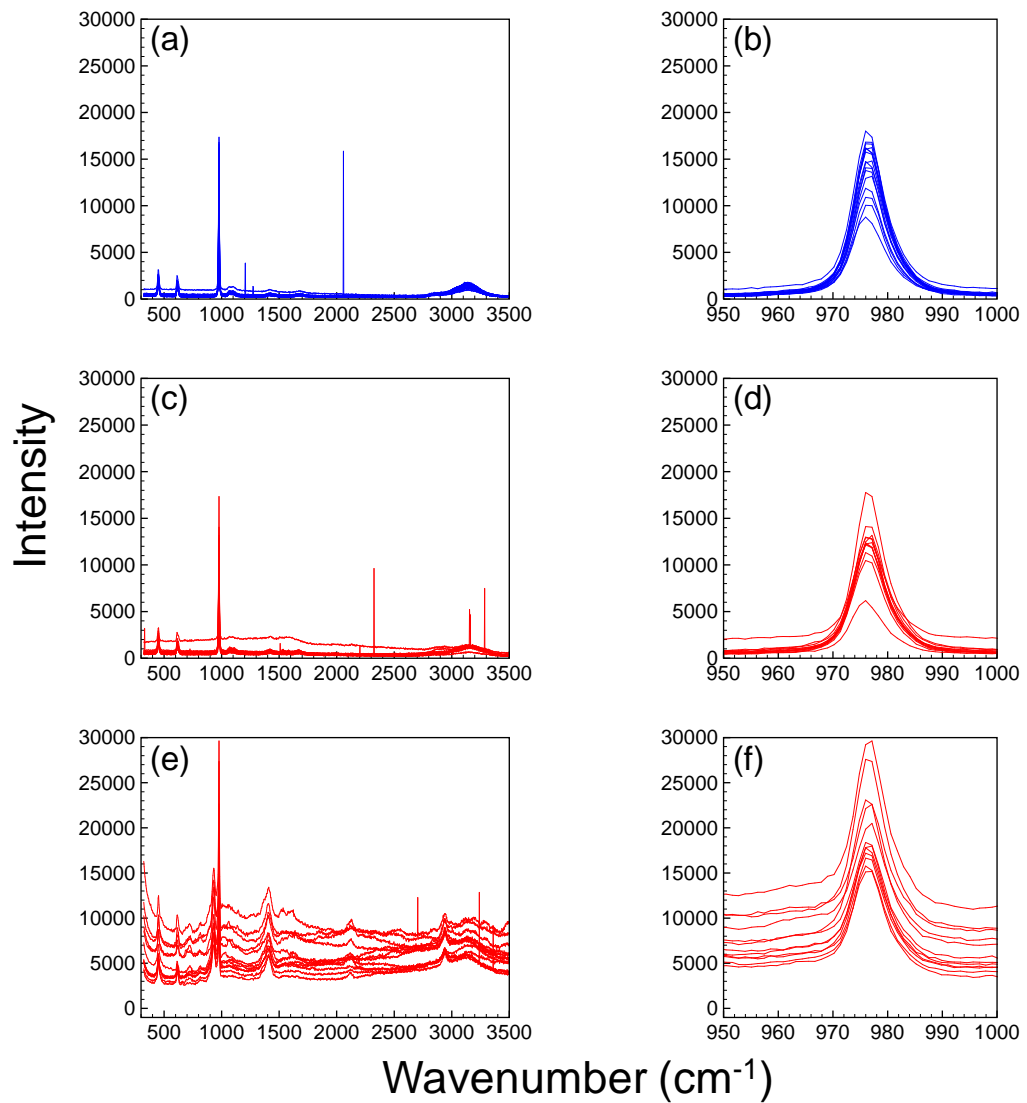
Figure S1. (a) Normal and (c, e) enhanced spectra of AS particles which were used for quantification of I_{SERS}/I_{NR}. (b, d, f) Magnified views of spectra at 950-1000 cm^{-1} corresponding to $v(SO_4^{2-})$. Note that in the presence of aggregated Ag nanoparticles, enhanced spectra (e) showed strong peaks of citrate at 2945, 1395, and 932 cm^{-1} corresponding to $v(C-H)$, $v(COO)$ and $v(C-COO)$, respectively.
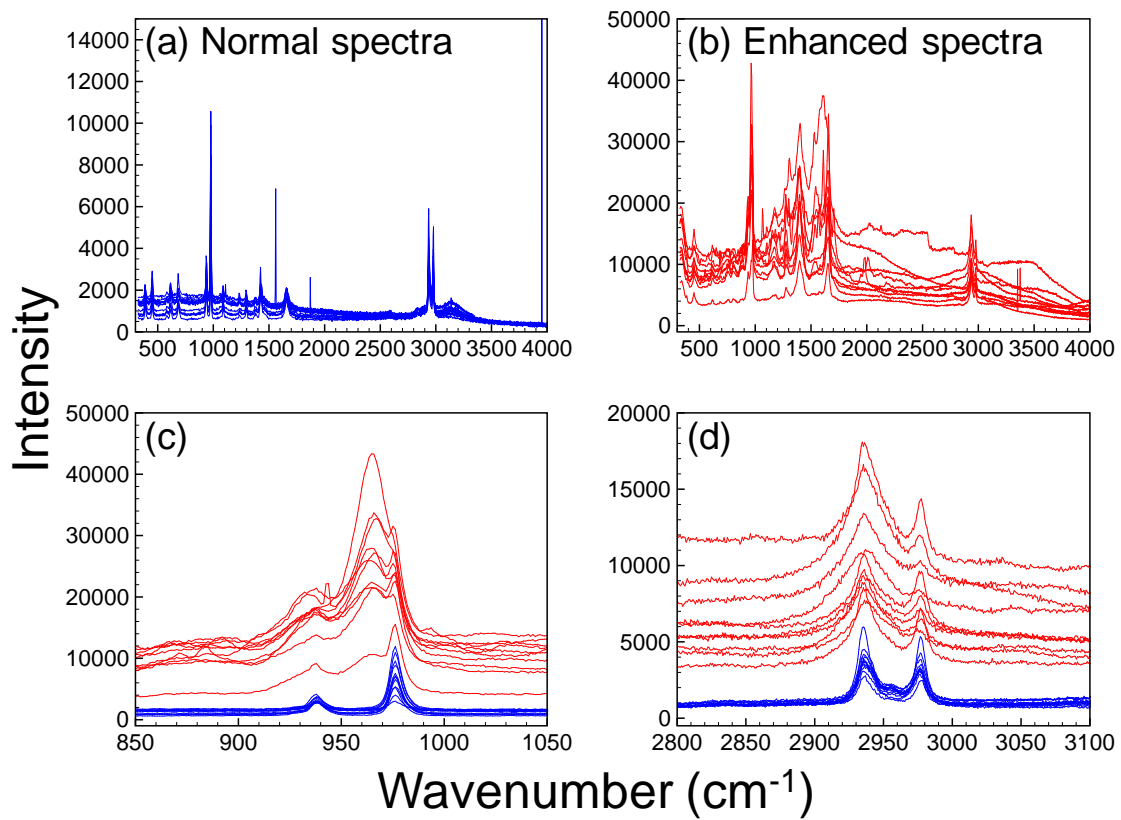
Figure S2. (a) Normal (blue) and (b) enhanced (red) spectra of AS/SA particles which were used for quantification of I_{SERS}/I_{NR}. (c, d) Magnified views of the corresponding spectra at 850-1050 and 2800-3100 cm^{-1} corresponding to $v(SO_4{}^{2-})$ and $\delta(OH\cdots O)$, and $v(C\text{-}H)$, respectively.
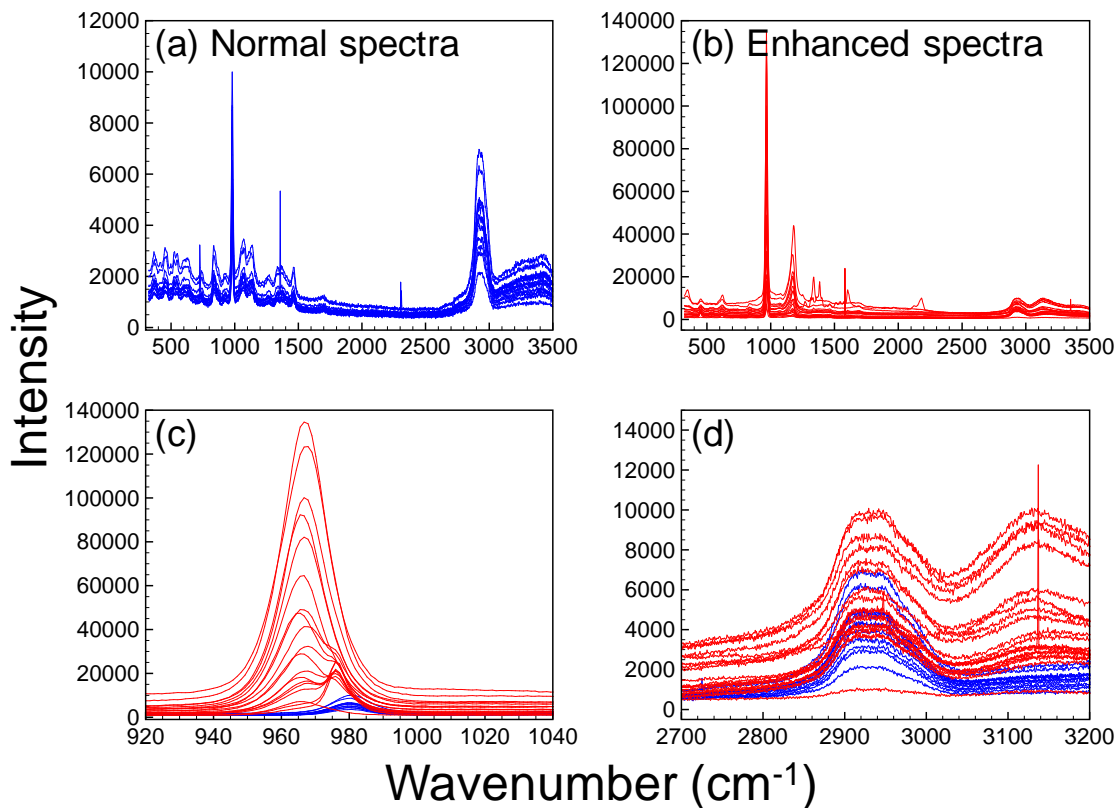
Figure S3. (a) Normal (blue) and (b) enhanced (red) spectra of AS/sucrose particles which were used for quantification of I_{SERS}/I_{NR}. (c, d) Magnified views of the corresponding spectra at 850-1050 and 2800-3100 cm^{-1} corresponding to $v(SO_4^{2-})$ and $v(C-H)$, respectively.

Comment #6: The use of the gold coating on the Si wafer needs to be described in more detail. It is unclear the purpose of this and whether it plays a role in the enhancements. If the enhancements are from the gold or partially gold and partially silver, this is important for the overall findings. More information would be helpful to evaluate this possibility. Do AS particles on just Si with Gold sputtered coating give any enhancements? It seems like an expensive choice if there is no specific reason for doing it, so a more convincing description would be helpful.

Response: Sulfate has a major peak in the range of 900-1000 cm^{-1}. We used gold coating on the Si wafer for masking peaks from the Si wafer such as at 520 (sharp) and 900-1000 (broad) cm^{-1}. Since Raman enhancement mainly comes from roughened surfaces or nanostructures, we believe that the gold coating on Si wafer (flat surface) does not significantly contribute to Raman enhancement, although the high reflectivity of gold coating may increase the light collection efficiency. We have added the following text in the section 2.1 in the revised manuscript:

"The gold coating was used to mask peaks of Si wafer at 520 and 900-1000 cm^{-1}."

Comment #7: Lines 153-160: For the nanoparticles no information is given about the size distribution and physical characteristics. The methods used are listed, but not the values for the silver nanoparticle synthesized. Given the importance of the silver nanoparticle properties for generating an enhanced response, more details are needed about what is being deposited on the atmospheric or model system particles. The journal EnvSci:Nano has a nice list of suggested nanoparticle characterization criteria that all papers using nanoparticles should us, this might be a good guide as to the detail that should be included in the manuscript. Similarly since the size distribution after electrospraying with the DMA and CPC would be helpful to evaluate whether particles are individual particles or aggregates after ESI.

Response: We have discussed the size distribution and physical characteristics (visible absorbance due to localized surface plasmon resonance) of Ag nanoparticles in the section 3.1. The size distribution after electrospraying in the gas phase has been added in Fig. S3 in the original supporting information. The electrosprayed Ag nanoparticles were not aggregates, because the mode size (Fig. S3) was generally consistent with the primary particle size and the size of nanoparticles deposited on the substrate. To make this clearer, we performed additional experiments on SEM observation of naturally dried suspension of Ag nanoparticles before electrospraying. The SEM observation shows the primary particle size of 56 nm. To address the reviewer's comment, we have added the following figure as Fig. S7 as well as the following text in the revised supporting information and manuscript (lines 253-257), respectively:

"The nanoparticles dried from the original suspension and those deposited (electrosprayed) on the gold-coated silicon substrate were observed with SEM as shown in Fig. S7 a and c, respectively. The size distribution of the deposited particles (Fig. S7 d) shows a peak of ~67 nm which is close to the primary particle size (56 nm in Fig. S7 b) and the particle size (53 nm in Fig. S6) of the aerosol from the electrospray."
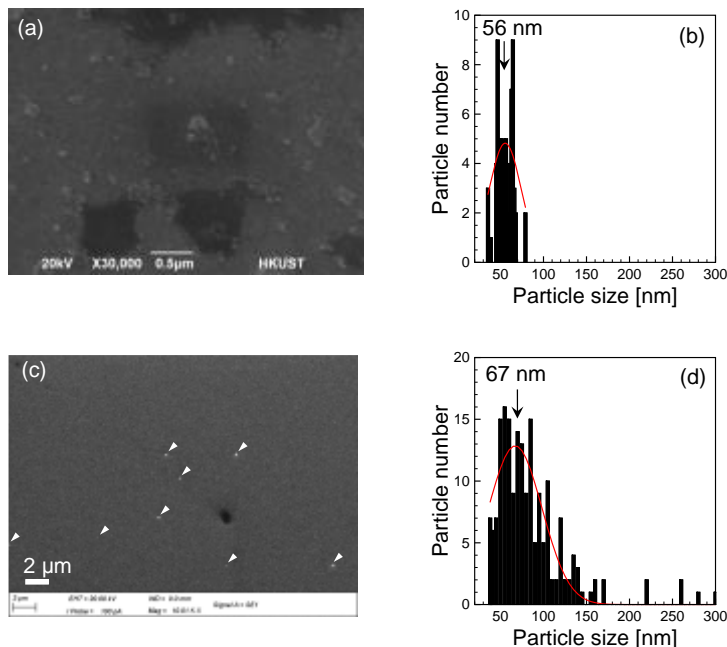
Figure S7. (a, c) SEM images of and (b, d) size distributions of Ag nanoparticles after naturally dried suspension and deposited (electrosprayed) on the substrate, respectively. Inset images shows typical SEM images. 71 and 208 particles were totally counted to obtain the size distributions for (b) and (d), respectively. The solid lines were fitted to normal distribution.

Comment #8: Lines 140-148: The aerosol size distribution also needs to be described in more detail. What was the size distribution of aeorsols. All of the information given is that the aerosols are generated and deposited (in the methods). Information like the mode, any size selection, etc would be very helpful in understanding the particle properties. Are the AS particles are assumed to be effloresced crystals since they are stored at < 10% RH and then analyzed at 60% (below the deliquescence RH of AS)? This could impact the enhancement of the SERS by determining nanoparticle/ammonium sulfate interacttions.

Response: (1) We assume that the Reviewer asked for the size distribution of analyte particles, because we have already shown the size distribution of Ag nanoparticle aerosols in the original supporting information (Fig. S3). In this study, we deposited analyte particles in the laboratory and collected ambient PM collected using a cascade impactor (Model MPS-4G1, California Measurements Inc.). We did not calculate the size distribution of the laboratory generated particles, but chose particles larger than 20 µm for most cases as mentioned in the section 2.4. For ambient PM, particles smaller 0.15 µm were selected to test the ES-SERS. To address the reviewer's comment, we have added the following text in the section 2.1 (lines 157-161) and changed the title accordingly:

"Ambient PM was collected on gold-coated Si substrates at the South Gate of the Hong Kong University of Science and Technology using a cascade impactor (Model MPS-4G1, California Measurements Inc.) on the morning of 9 May 2016. Collected particles between 0.05 and 0.15 µm in aerodynamic diameter were used as analyte particles."

(2) Since AS particles have effloresced before the RH was set at 60%, no enhancement was observed, likely because of the weak interaction between ammonium sulfate and Ag nanoparticles. In contrast, the aqueous AS/sucrose particles at 60% RH showed the significant enhancement at the sulfate vibration mode (Fig. 3), suggesting the strong interaction.

Comment #9: For the enhancement (162) reported on line 354, what size particles does this refer to? Is it possible that a larger particle versus a smaller particles is playing a role? This is part of why more details are needed for the aerosol sizing.

Response: The size of AS/sucrose particle is 1.4 µm for the I_{SERS}/I_{NR} of 162. To make this clearer, we have revised the corresponding text accordingly:

Revised text:
Hence I_{SERS}/I_{NR} increases with decreasing size, resulting in the largest I_{SERS}/I_{NR} of 162.0 for the $\nu(SO_4^{2-})$ mode at a particle size of 1.4 µm.

No clear role of analyte particle size in Raman enhancement was observed for laboratory-generated particles (Fig. 6). As discussed in the second paragraph in the section 3.3, this is because Ag nanoparticles are deposited on the surface of analyte particles and the surface area irradiated by a laser was constant over the size range studied (1.4 ~ 40 µm) due to the smaller laser spot diameter (1 µm). If the size of analyte particle is smaller than a laser sport diameter, enhanced intensity probably decreases with the size of analyte particles. However, the above discussion cannot be extended to the result of ambient PM (< 0.15 µm) collected by impactors,

which were concentrated onto a submillimetre-sized spot area on the substrate during impaction.

Minor comments

Comment #1: Line 80: The Ofner paper referenced is of TERS, which while similar to SERS, should be specifically noted as such.

Response: We agree. We have accordingly revised the corresponding text as follows:

"Recently surface enhanced and Raman spectroscopy (SERS) and tip enhanced Raman spectroscopy (TERS) have been applied for characterizing atmospheric particles (Craug et al., 2015; Ofner et al., 2016)."

Comment #2: Line 329-331: The depth of focus section is not clear and should be discussed in more detail.

Response: We have revised and added the following text:

"This estimated value is smaller than the nominal threshold of 10 µm observed in the size dependence of the normal Raman signals, because gravity had affected the shape of the analyte particles deposited on the substrate, reducing the particle height (<10 µm). Gravity deforms the shape of droplets on a substrate, when the size of droplet is sufficiently large (e.g. > 10 µm). A contact angle of large droplet to a substrate is much smaller than 180 degrees. Thus, the depth of substrate-deposited droplet is typically smaller than its diameter."

Comment #3: More details on Gen and Lenggoro method need to be added.

Response: We have added the following text in the introduction (lines 110-116):

"They employed the electrospray deposition of positively charged Ag nanoparticles on a silicon wafer that had been dip-coated with an organic thin film. The concentration of the organics on the substrate ranged from ~1 to 30 nanograms/m^2. The Raman mapping allows direct measurement of a spatial distribution of organic molecules on a solid surface with the detection limit above 3.54 molecules/µm^2. Numerical electrodynamic simulations have revealed that singly charged Ag nanoparticles (50 nm) can be deposited on any surface, i.e., from metallic to non-metallic substrates, under an electric field of > 10^4 V/m."

Comment #4: Figure 4: It would be nice to see the rest of the Raman spectrum (perhaps as an inset) to evaluate any nanoparticle effects.

Response: We have added the entire Raman spectra in Figures S1, S2 and S3 in the revised supporting information.

Comment #5: Figure 6: Why does the peak shift to lower frequencies? More information on this would be helpful.

Response: This redshift is likely due to strong interaction between sulfate ion and Ag nanoparticles, as reported by earlier works (Campion and Kambhampati, 1998; Stockle et al., 2000) and described in the second paragraph in the section 3.2.

Comment #6: Figure 7: For the particles that is very weak signal for very large particles. What is the RH of the particles when analyzed? Is it really safe to assume they are aqueous? Many prior Raman aerosol paper show much sharper sulfate features for ambient particles, why does the SERS struggle here so much?

Response: The RH during Raman analysis was 60 %. More importantly, the particles were dried at RH = 10% before they were conditioned at 60%. Hence, the AS and AS/succinic acid particles were solid in the current study. Nonetheless, enhanced spectra showed water peaks at 3200-3500 cm^{-1}, which are attributed to surface adsorbed water. As shown in Figs. 3 and 4, we observed sharp sulfate peaks at ~980 cm^{-1}.

Comment #7: Figure 8: Why is the ν(O-H) stretching region not shown? - This is a minor point, but the figures take a very long to load, which I would guess is related to the resolution used. Please check that the figures load easily for a future draft (hopefully this is not just my computer having issues).

Response: We have revised Fig. 8 (Fig. 10 in the revised manuscript) to show the entire Raman spectra. We have reduced the data size of the figure.

Reference:

Campion, A., and Kambhampati, P.: Surface-enhanced Raman scattering, Chem. Soc. Rev., 27, 241-250, doi: 10.1039/a827241z, 1998.

Dieringer, J. A, McFarland, A. D., Shah, N. C., Stuart, D. A., Whitney, A. V., Yonzon, C. R., Young, M. A., Zhang, X., and Van Duyne, R. P.: Surface enhanced Raman spectroscopy: new materials, concepts, characterization tools, and applications, Farad. Discuss., 132, 9-26, doi: 10.1039/B513431P, 2006.

Fu, Y., Kuppe, C., Valev, V. K., Fu, H., Zhang, L., and Chen, J.: Surface-enhanced Raman spectroscopy: A facile and rapid method for the chemical component study of individual atmospheric aerosol, Environ. Sci. Technol, 51, 6260-6267, doi: 10.1021/acs.est.6b05910, 2017.

Le Ru, E. C., Blackie, E., Meyer, M., and Etchegoin, P. G.: Surface enhanced Raman scattering enhancement factors: A comprehensive study, J. Phys. Chem. C, 111, 13794-13803, doi: 10.1021/jp0687908, 2007.

Munro, C. H., Smith, W. E., Garner, M., Clarkson, J. W. P. C., and White, P. C.: Characterization of the surface of a citrate-reduced colloid optimized for use as a substrate for surface-enhanced resonance Raman scattering, Langmuir, 11, 3712-3720, doi: 10.1021/la00010a021, 1995.

Schmidt, M. S., Hübner, J., and Boisen, A.: Large area fabrication of leaning silicon nanopillars for surface enhanced Raman spectroscopy, Adv. Mater., 24, OP11-OP18, doi: 10.1002/adma.201103496, 2012.

Stöckle, R. M., Suh, Y. D., Deckert, V., and Zenobi, R.: Nanoscale chemical analysis by tip-enhanced Raman spectroscopy, Chem. Phys. Lett., 318, 131-136, doi: 10.1016/s0009-2614(99)01451-7, 2000.

Response to Reviewer #2

Authors present ES-SERS approach to characterize atmospheric aerosol particles. This is not a new approach, but new in terms of application as this is not been applied to atmospheric particles in the past. It seems such approach can be applied to atmospheric aerosols, and results are encouraging. Such approach was also recently published (El-Khoury, Johnson et al. 2015), therefore this is not a new approach and manuscript should be modified to reflect this. I have few major comments, and after these are addressed, I recommend the manuscript for publication.

Response: We thank you for useful comments. The earlier paper referred by reviewer #2 mentioned (El-Khoury, Johnson et al., 2015) utilized electrospray deposition of "analyte" solutions **onto 2-dimensional array of silver nanospheres on an SERS substrate**, which is a conventional approach of using a SERS substrate (Fig. 1a in the main text). In contrast, our approach (Fig. 1b in the main text) uses electrospray for generating and depositing Ag nanoparticles (SERS-active agent) onto the analyte atmospherically relevant particles. With our current approach, we will be able to characterize surface chemical composition of particles. Revised and added text in the main manuscript and supporting information was highlighted in red.

Comment #1: To simplify the reading, I suggest authors revise the particle definition terminology. It is confusing as aerosols are typically defined in the sense that these are the particles that are present in the atmosphere and affect Earth's radiative properties (optical and cloud). In this paper aerosol is defined as silver nanoparticles, and conventionally defined aerosol as 'analyte particles.' Please revise such that these analyte particles are now called aerosols and Ag nanoparticles as Ag nanoparticle only. Defining Ag nanoparticles as aerosol is confusing.

Response: We thank you for the comment. We agree that describing Ag nanoparticles as aerosol is confusing. To address the reviewer's comment, we have revised the terminology throughout the entire manuscript accordingly.

Comment #2: It is not clear why sucrose compound was used? Does this represent atmospheric organic aerosol composition? Please provide some references. Please clarify the necessary to

coat the silicon wafer with gold. Are these wafers home grown or commercially available (part number? and vendor?).

Response: (1) Sucrose is widely used as a surrogate of viscous compound in the atmospheric aerosol community. We have accordingly provided the reference and added the following text in the section 2.1 (lines 148-150).

"In this study, atmospherically relevant particles of AS, AS mixed with SA, and AS mixed with sucrose were examined (Ling and Chan, 2008; Zobrist et al., 2008; Freedman et al., 2010; Chu and Chan, 2016)."

(2) The purpose of gold coating was to mask sharp and broad peaks derived from Si wafer at 520 and 900-1000 cm^{-1}, respectively. We have accordingly added the following text (lines 156-157):

"The gold coating was used to mask peaks of Si wafer at 520 and 900-1000 cm^{-1}."

(3) The Si wafers used are commercially available (100, N type, Y Mart, Inc).

Comment #3: In section 2.2 it is mentioned that SEM images were obtained. Can they be inserted into the main paper? Why UV-vis was used? Describe typical CPC concentration values. What was the size of Ag nanoparticles (53 nm?) that was size-selected.

Response: (1) We prefer to keep the SEM images in the supporting information, because these are not our main results. Instead, we have inserted two figures of SERS results (Figs. S5 and S6) into the main manuscript to improve the readability in response to the reviewer's comment #7.

(2) UV-vis spectrometer was used for characterizing the selective absorption of Ag nanoparticles in liquid phase (colloidal suspension) as shown in Fig. S2. SERS relies on the excitation of localized surface plasmon resonance of metalic nanoparticles resulting in the selective absorption.

(3) CPC was used to obtain the size distribution of Ag nanoparticles suspended in gas phase. To address the reviewer's comment, the y axis of figure S3 was represented as particle number concentration (particles/cm^3). The typical CPC concentration was 40 to 50 particles/cm^3 at the mode size.

(4) We did not size-select the Ag nanoparticles. We have calculated the size (mode number) of 53 nm from the size distribution of Ag aerosols obtained with DMA and CPC (Fig. S3).

Comment #4: How spraying time of 1 hour was determined.

Response: The spraying time of 1 hour was determined based on earlier work (Gen and Lenggoro, 2015). The electrospray system used in the current study has a similar configuration with the system used in the earlier work. As mentioned in the introduction, we developed the

ES-SERS method following the earlier work. To address the reviewer's comment, we have revised the corresponding text accordingly (lines 192-194):

"Ag nanoparticles were deposited on the substrate at ambient pressure (1 atm) and the spraying time was 1 hour based on earlier work (Gen and Lenggoro, 2015)."

Comment #4: Model name and software version of the Renishaw Raman microscope should be mentioned. Please specify wavenumbers corresponding to compounds specified on line 198 (page 8).

Response: The software name and wavenumbers have been added in the section 2.4 as follows:

"Instrument control was performed with the Renishaw WiRE (Renishaw)."

"Raman enhancement was observed for vibration modes of $v(SO_4^{2-})$, $v(NO_3^-)$, v(C-H), and v(O-H) at ~970, ~1034, ~2930 and 3200 ~ 3500 cm^{-1}, respectively."

Comment #5: Section 2: Please mention here how submicron ambient aerosol were collected in this section. It is already mentioned in section 3.5. How particles between 0.05 and 0.15 um were collected. Using impactor? What stage and what was the 50% cut size. How samples were dried? And why it was necessary to dry the particles. Can drying process could alter the surface composition? Do you have Raman maps for ambient particles?

Response: (1) We used a cascade impactor (Model MPS-4G1, California Measurements Inc.) and selected the last stage where the 50% cut size is between 0.05 and 0.15 µm, which was described in the section 3.5. We have moved the description from the section 3.5 to section 2.1.

(2) The samples were kept in a desiccator filled with silica gels. This process dried the samples, which could vaporize some volatile organic compounds.

(3) We don't have Raman maps for ambient particles, because the particle size (< 0.15 µm) is below the spatial resolution of Raman analysis (~ 1 µm) and it also runs into the light diffraction limit.

Comment #6: Section 3.2: It is bit confusing to understand the comparison between Ag-coated SERS substrate and current SERS method. Why this comparison is carried out? In both cases the test aerosol are similar, so I expect the spectra from both methods should be similar. In terms of intensity, it can be just coincidence. It also raises important question, if both methods yield similar results, why one should use ES-SERS technique. One can use commercially available SERS substrates, which can save a lot of time in regards to sample preparation. Any thoughts? This result also contradicts the advantages of ES-SERS described in Introduction section.

Response: This comparison was carried out to examine the effect of Ag-sulfate interaction on Raman peaks, particularly the sulfate peaks (i.e. ~980 cm^{-1}). We observed a redshift at the sulfate peak for the ES-SERS experiments. The same redshift was also observed using the Ag-

coated SERS substrate, suggesting that the results with the ES-SERS were not due to experimental error.

Unlike the conventional technique using an SERS substrate, our ES-SERS yields information on surface chemical compositions of analyte particles. If there are concentration gradients of species in radial direction in an analyte particle, the resulting spectra obtained from the two methods would be different. It is apparent that enhanced spectra from two cases (1) ES-SERS (Ag nanoparticles on the top of analyte particles) and (2) conventional SERS substrate (the nanoparticles underneath analyte particles) come from the different positions of the particles. SERS is a type of surface spectroscopy, which means that only the analyte molecules adsorbed to Ag nanoparticles contribute to the enhancement and its effect is the distance dependence (Dieringer et al., 2006). Therefore, ES-SERS is more sensitive to the surface of the analyte particles and is useful for surface characterization of atmospheric particles.

We have compared our results with earlier works. We have added the following text and revised the corresponding text accordingly (lines 389-397):

"Craig et al. (2015) reported an enhancement factor of 2.0 at $v(SO_4^{2-})$ mode of ~970 cm^{-1} using an SERS substrate with the AS particles on the top of Ag nanoparticles on the substrate. Furthermore, Fu et al. (2017) reported an enhancement factor of 6.1 for the same mode, using commercial SERS substrates with pre-determined gold-coated structure of inverted pyramids (Klarite, Renishaw Diagnostics Ltd.). Our results of AS/sucrose particles (Table 1) showed that the I_{SERS}/I_{NR}, which is the lower limit of enhancement factor, ranged from 12.4 to 163, much higher than the above studies. Note that I_{SERS}/I_{NR} is the lower limit of the enhancement factor ($I_{SERS}N_{vol}/I_{NR}N_{surf}$) conventionally used because N_{vol}/N_{Surf} is much greater than unity in the present case."

Comment #7: Section 3 in general. One has to go back and forth between the main paper and supplementary information to understand the results. I suggest if some figures can be inserted into the main paper to improve the readability.

Response: We have moved Figs. S6 and S7 into the main text.

Comment #8: Section 3.3: Line 314-316. Is this observed in this study? and how such distance is determined? Are there any SEM images that shows such information.

Response: This distance dependence is a well-known result from Dieringer et al. (2006), also cited in the main text. We have discussed the size effect in this section based on the fact. Unfortunately, we don't have SEM images to show such information.

Comment #9: Line 332: To improve readability I suggest to add the values of wavelength and NA.

Response: We thank you for the comment. We have accordingly added the values.

Comment #10: Line 334: ..'gravity had affected..' is not clear. How gravity affects the shape. Shape (morphology) can be also altered during impaction.

Response: Gravity deforms the shape of droplets on a substrate and makes a contacting area between a droplet and a substrate larger, when the size of droplet is sufficiently large (e.g. > 10 μm). Therefore, substrate-deposited large droplets are not perfectly spherical; in other words, the contact angle is much smaller than 180 degree. Based on this, the height of droplet is always smaller than its diameter for large droplets. We have revised the text as follows (lines 365-371):

"This estimated value is smaller than the nominal threshold of 10 μm observed in the size dependence of the normal Raman signals, because gravity had affected the shape of the analyte particles deposited on the substrate, reducing the particle height (<10 μm). Gravity deforms the shape of droplets on a substrate, when the size of droplet is sufficiently large (e.g. > 10 μm). A contact angle of large droplet to a substrate is much smaller than 180 degree. Thus, the depth of substrate-deposited droplet is typically smaller than its diameter."

Comment #11: Line 347-348: Please mention what components were observed in minor and major category.

Response: Since Ag nanoparticles sit on the top of analyte particles, we define minor and major components as non-enhanced and enhanced ones, respectively. The non-enhanced and enhanced components reflect bulk chemical composition and surface chemical composition, respectively. To avoid confusion, we have deleted the descriptions of "minor" and "major" and revised the corresponding text as follows:

"Considering these facts, the constant enhanced intensity provides evidence that the enhanced spectrum contains information about the bulk chemical compositions (non-enhanced component) as well as the surface compositions (enhanced component), making the ES-SERS technique suitable for surface-sensitive detection."

Comment #12: Line 427:429: It is bit confusing. Does this imply that ES-SERS can only give surface composition but not bulk.

Response: The ES-SERS gives both bulk and surface information of chemical compositions, but only the surface compositions are enhanced due to the distance-dependence nature of SERS. Once we have a normal spectrum that contains only the bulk information, we will be able to extract the surface information by comparing a SERS spectrum with a normal spectrum. To clearly state those, we have added the following text:

"The spectrum obtained from ES-SERS contains both bulk and surface information of chemical compositions, but only the surface compositions are enhanced due to the distance-dependence effect (Dieringer et al., 2006). The complementary methods of Raman spectroscopy and ES-SERS (as surface-sensitive spectroscopy) can provide the bulk and surface chemical compositions, respectively by comparing normal and enhanced Raman spectra. They potentially help reveal the internal structure of individual particles such as their core/shell structure."

Comment #13: Line 428: 'comma' after word composition is missing. ....compositions, respectively,. . ..

Response: Thanks for the comment. We have accordingly added the comma.

Comment #14: Section 4: Please revise this section. Remove any new material that is not discussed in the main text. Remove any speculations or theories. Discuss them in the main text. Some editorial work is needed to understand the main message of the paper. Main conclusions are not clear after reading this section. Please see below some comments to improve this section further.

Response: Based on the reviewer's comment, we have revised and removed some text as below.

Comment #15: Line 433: This is not a new technique. Rephrase the sentence.

Response: We think that our method is a new technique as the publication referred by the reviewer is different from ours. Therefore, we prefer not to rephrase the sentence.

Comment #16: Line 436-439: Sentence is not clear. Cannot understand the phrase, please rewrite.

Response: To address the reviewer's comment, we have revised the sentence as follows:

"ES-SERS measurements showed that the I_{SERS}/I_{NR} ratios of the $v(SO_4^{2-})$ band at ~970 cm^{-1} for laboratory-generated AS, AS/SA and AS/sucrose particles followed the order: AS/sucrose (I_{SERS}/I_{NR} = 12.4) > AS/SA (I_{SERS}/I_{NR} = 3.3) > AS (I_{SERS}/I_{NR} = 1)."

Comment #17: Line 447-449: To improve readability, I would move this sentence to the main text. These past studies are not discussed either. Please discuss these. DMA is already defined for differential mobility analyzer (line 159).

Response: We thank you for the comment. We have removed the following text to improve the readability of this section:

"Adsorbed water has been investigated by limited techniques such as Fourier transform infrared spectroscopy (Al-Hosney and Grassian, 2005) and differential mobility analyzers (Romakkaniemi et al., 2001), which provide direct and indirect observations, respectively. ES-SERS can also contribute to elucidating the role of surface-adsorbed water in future studies."

Comment #18: Line 465-466: This is new and speculative. Please move to the main text and discuss. Do you have any maps that support this premise? Check (Baustian, Cziczo et al. 2012) for further information regarding maps and morphology.

Response: (1) This is not a new statement. We have already discussed this in line 421 in the original main text.

(2) We don't have Raman maps to support the premise. The earlier paper referred by the reviewer used Raman mappings for particles larger than 1 μm. The size of ambient particles discussed here (in the line 465) is below 1 μm (0.05 and 0.15 μm). Such maps may not give the detailed information on morphology in the current study.

Comment 19 #: Line 467-472: Paragraph text is confusing. How this is relevant to the present study. I suggest delete or modify and move to the main text.

Response: In this paragraph, we would like to describe (i) some limitations of ES-SERS that need further studies and (ii) a possible solution to overcome the limitations. We have revised this paragraph as follows:

"The direct contact of Ag nanoparticles to analyte molecules results in a peak shift, which could pose an obstacle to tracing the phase transition as well as identifying functional groups of the analytes. Recent studies have introduced the use of core-shell composite gold nanoparticles to eliminate the chemical enhancement (Li et al., 2010; Li et al., 2013). The outermost inert shell layer of the nanoparticle prevents its direct contact (i.e. coupling) with analyte molecules. Using such novel nanoparticles could further extend the application of the proposed ES-SERS technique in atmospheric studies."

Comment #20: Figure 8: In caption mention the wavenumber corresponding to sulfate and organics. How Organics peaks were identified?

Response: The enhanced Raman spectrum shows a peak at 1777 cm^{-1} that is likely assigned to carbonyl group, indicative of organic components. This explanation was described in the line 414 in the original main text. To make this clearer, we have revised the caption as follows:

"**Figure 10**. Normal (blue) and enhanced (red) Raman spectra of ambient PM. The particle size is between 0.05 and 0.15 µm. Sulfate peaks at 451, 615 and 977 cm^{-1}, and D and G bands at 1341 and 1598 cm^{-1}, respectively, were observed. Enhanced spectra further showed peaks at 1039 (nitrate) and 1777 (carbonyl group, indicative of organic components) cm^{-1}. The illustrations (not to scale) present experimental configurations for normal Raman and SERS measurements. The normal spectrum includes the bulk chemical compositions of BC and sulfate and the enhanced one includes the bulk compositions as well as the surface compositions (i.e. sulfate and organics)."

Reference:
Chu, Y., and Chan, C. K.: Reactive uptake of dimethylamine by ammonium sulfate and ammonium sulfate–sucrose mixed particles, J. Phys. Chem. A, 121, 206–215, doi: 10.1021/acs.jpca.6b10692, 2016.

Dieringer, J. A, McFarland, A. D., Shah, N. C., Stuart, D. A., Whitney, A. V., Yonzon, C. R., Young, M. A., Zhang, X., and Van Duyne, R. P.: Surface enhanced Raman spectroscopy: new materials, concepts, characterization tools, and applications, Farad. Discuss., 132, 9-26, doi: 10.1039/B513431P, 2006.

Freedman, M. A., Baustian, K. J., Wise, M. E., and Tolbert, M. A.: Characterizing the morphology of organic aerosols at ambient temperature and pressure. Anal. Chem., 82, 7965-7972, doi: 10.1021/ac101437w, 2010.

Gen, M., and Lenggoro, I. W.: Probing a dip-coated layer of organic molecules by an aerosol nanoparticle sensor with sub-100 nm resolution based on surface-enhanced Raman scattering, RSC Adv., 5, 5158-5163, doi: 10.1039/c4ra03850a, 2015.

Ling, T. Y., and Chan, C. K.: Partial crystallization and deliquescence of particles containing ammonium sulfate and dicarboxylic acids, J. Geophys. Res., 113, D14205, doi: 10.1029/2008jd009779, 2008.

Zobrist, B., Marcolli, C., Pedernera, D. A., and Koop, T.: Do atmospheric aerosols form glasses?, Atmos. Chem. Phys., 8, 5221-5244, doi: 10.5194/acp-8-5221-2008, 2008.

1 **Electrospray-Surface Enhanced Raman Spectroscopy (ES-SERS) for**

2 **probing surface chemical compositions of atmospherically relevant particles**

4 Masao Gen and Chak K. Chan*

6 School of Energy and Environment, City University of Hong Kong, Tat Chee Avenue,

7 Kowloon, Hong Kong, China

8 *E-mail: chak.k.chan@cityu.edu.hk. Phone: +(852)-3442-5593. Fax: +(852)-3442-0688.

Abstract

We present electrospray-surface enhanced Raman spectroscopy (ES-SERS) as a new approach to measuring the surface chemical compositions of atmospherically relevant particles. The surface-sensitive SERS is realized by electrospraying Ag nanoparticle aerosols over analyte particles. Spectral features at $\nu(SO_4^{2-})$, ν(C-H) and ν(O-H) modes were observed from the normal Raman and SERS measurements of laboratory-generated supermicron particles of ammonium sulfate (AS), AS mixed with succinic acid (AS/SA) and AS mixed with sucrose (AS/sucrose). SERS measurements showed strong interaction (or chemisorption) between Ag nanoparticles and surface aqueous sulfate $[SO_4^{2-}]$ with $[SO_4^{2-}]_{AS/sucrose} > [SO_4^{2-}]_{AS/SA} > [SO_4^{2-}]_{AS}$. Enhanced spectra of the solid AS and AS/SA particles revealed the formation of surface-adsorbed water on their surfaces at 60% relative humidity. These observations of surface aqueous sulfate and adsorbed water demonstrate a possible role of surface-adsorbed water in facilitating the dissolution of sulfate from the bulk phase into its water layer(s). Submicron ambient aerosol particles collected in Hong Kong exhibited non-enhanced features of black carbon and enhanced features of sulfate and organic matter (carbonyl group), indicating an enrichment of sulfate and organic matter on the particle surface.

1. Introduction

53 Atmospheric aerosols are emitted from a variety of sources and complex mixtures of organic

54 and inorganic substances (Ault and Axson, 2017). Due to the complex components, aerosols

55 have a wide range of physical and chemical properties (Hinds, 1999; Sullivan and Prather,

56 2005; Ault and Axson, 2017). Aerosols affect both the climate and human health on a global

57 scale (IPCC, 2013; Pope and Dockery, 2006). They scatter and absorb solar radiation and alter

58 the properties of clouds, potentially affecting radiative transfer and precipitation behaviors

59 (IPCC, 2013; DeMott et al., 2016). Exposure to particulate matter (PM) has adverse effects on

60 cardiopulmonary health (Pope and Dockery, 2006).

61 Thin film water is ubiquitous and can cover the surfaces of many materials (Ewing,

62 2006). Earlier work has reported the formation of a monolayer of adsorbed water on the surface

63 of solid AS at 60% relative humidity (RH) (Romakkaniemi et al., 2001). Surface-adsorbed

64 water plays a potential role in facilitating the heterogeneous chemistry of atmospheric aerosols

65 (Trainic et al., 2012; Chu and Chan, 2016). Yet the relative role of surface chemistry and bulk

66 processes is poorly understood due to the lack of surface-sensitive techniques available for

67 studying individual atmospheric particles (Ault et al., 2013).

68 Spectroscopic methods, particularly Raman spectroscopy, are useful for investigating

69 the physical properties and chemical components of complex atmospheric particles. Raman

70 studies have been carried out to probe the phase state (Bertram et al., 2011), hygroscopic

71 properties (Yeung et al., 2009), and heterogeneous reactivity (Lee and Chan, 2007) of

72 laboratory-generated atmospherically relevant particles at precisely controlled RHs. However,

73 Raman measurements of atmospherically relevant particles have been limited to the highly

74 Raman-active modes of $v(SO_4^{2-})$ (Yeung et al., 2009), $v(NO_3^-)$ (Lightstone et al., 2000), v(C-

75 H) (Chu and Chan, 2016) and black carbon (BC) (Sze et al., 2001), due to insufficient

76 sensitivity to other modes. In addition, Sobanska et al. (2012) reported a strong fluorescence

77 signal from the humic substances in clay mineral aerosols, which can mask Raman signals

78 (Sobanska et al., 2012). Expanding the detection range of Raman as well as enhancing Raman

79 signals can help elucidate particle phase processes occurring in the atmosphere.

80   Recently surface enhanced Raman spectroscopy (SERS) and tip enhanced Raman

81 spectroscopy (TERS) have been applied for characterizing atmospheric particles (Craig et al.,

82 2015; Ofner et al., 2016). SERS has the potential to overcome the limitations of insufficient

83 sensitivity and spatial resolution in conventional Raman spectroscopy. The technique relies on

84 the localized surface plasmon resonances in noble metal nanoparticles (e.g. silver and gold) to

85 trigger Raman enhancement (Jeanmaire and Van Duyne, 1977; Albrecht and Creighton, 1977).

86 Raman signals can be enhanced by up to 10^{10} times (Le Ru et al., 2007). Earlier works detected

87 not only the highly Raman-active modes but also other important modes such as v(C-C), v(C-

88 N), v(C=O) and v(O-H) modes in atmospheric particles (Craig et al., 2015; Ofner et al., 2016).

89 Craig et al. (2015) made use of SERS substrates coated with silver (Ag) nanoparticles for

90 collection of ambient or analyte particles (Craig et al., 2015). Despite the successful

91 enhancement of Raman signals within individual analyte particles, approaches using SERS

92 substrates may not be able to detect the surface chemical compositions of particles. This

93 limitation is attributable to the configuration of SERS active spots that are formed between the

94 SERS substrate and the analyte particle.

95   In most microscopic Raman studies, backscattered Raman signals of analyte particles

96 are collected in a microscopic configuration. When the analyte particles are deposited on the

97 Ag-coated SERS substrate (Craig et al., 2015), SERS active spots are located beneath the

98 particles. In other words, the photons must pass through the particle with a refractive index

99 greater than air, which would scatter/absorb light and reduce the signals received by the Raman

100 microscope. Furthermore, the SERS-substrate method collects enhanced Raman signals from

interfaces between the substrate and deposited particles but not the gas/particle interfaces, which are important for heterogeneous processes. A significant enhancement was observed only at the edge of particles likely due to spatially non-uniform SERS active spots distributed across individual particles (Craig et al., 2015).

Gen and Lenggoro (2015) recently developed an SERS approach to probe surfaces coated with an organic thin film by electrospraying Ag nanoparticle aerosols over the probed surfaces (Gen and Lenggoro, 2015). A number concentration of 11.6 particles/μm^2 and a narrow distribution of separation distance between deposited particles peaking at 100 nm confirmed the concentrated and uniform deposition pattern of Ag nanoparticles on a substrate respectively. They employed the electrospray deposition of positively charged Ag nanoparticles on a silicon wafer that had been dip-coated with an organic thin film. The concentration of the organics on the substrate ranged from ~1 to 30 nanograms/m^2. The Raman mapping allows direct measurement of a spatial distribution of organic molecules on a solid surface with the detection limit above 3.54 molecules/μm^2. Numerical electrodynamic simulations have revealed that singly charged Ag nanoparticles (50 nm) can be deposited on any surface, i.e., from metallic to non-metallic substrates, under an electric field of $> 10^4$ V/m. Following that approach, we devise an SERS technique to detect the surface chemical compositions of deposited analyte particles by creating uniform SERS active spots on the particle surface. Figure 1 shows a comparison of approaches using an SERS substrate with pre-deposited metal nanoparticles and our proposed method of depositing metal nanoparticle aerosols on collected analyte particles. Deposition of metal nanoparticle aerosols on an analyte particle creates SERS active spots on the surface of the analyte particle facing the microscope, similar to the TERS configuration (Uzayisenga et al., 2012; Yang et al., 2009) and therefore the photons from the enhancement can be directly transferred to a detector without passing through the analyte particle.

126   Aerosol technology has been used to generate aerosols with a wide range of sizes across

127   five orders of magnitude (Hinds, 1999; Okuyama and Lenggoro, 2003; Jaworek, 2007). Among

128   the techniques, the electrospray technique is a unique method that atomizes liquid using

129   electrical forces (de la Mora, 2007). It can produce submicron highly charged droplets, thus

130   preventing their coagulation and facilitating their self-dispersion. After solvent evaporation,

131   dried aerosols form rapidly at ambient temperatures and pressure. Since charges on droplets

132   can remain in dried aerosols, the motion of highly-charged dried aerosols can be precisely

133   controlled using electric fields (Kim et al., 2006; Lenggoro et al., 2006).

134   We report for the first time a technique called electrospray-SERS (ES-SERS) which is

135   designed to probe atmospherically relevant particles. We employ the electrospray technique to

136   deposit Ag nanoparticles on analyte particles. We present ES-SERS experiments on laboratory-

137   generated supermicron particles of ammonium sulfate (AS), AS mixed with succinic acid (SA)

138   and AS mixed with sucrose (AS/sucrose). The dependence of Raman enhancement at the

139    $v(SO_4^{2-})$ mode on surface sulfate anions is discussed. Effects of analyte particle size on Raman

140   signals are investigated with aqueous AS/sucrose particles. We then describe the direct

141   observation of surface adsorbed water on solid AS and AS/SA particles from enhanced Raman

142   signals of $v(O-H)$ mode. Lastly, we apply the technique to examine submicron ambient

143   particles.

144

145

146   **2. Experimental**

147   **2.1. Materials and sample preparation**

148   In this study, atmospherically relevant particles of AS, AS mixed with SA, and AS mixed with

149   sucrose were examined (Ling and Chan, 2008; Zobrist et al., 2008; Freedman et al., 2010; Chu

150   and Chan, 2016). AS (Sigma-Aldrich) and sucrose (Affymetrix USB Products) were dissolved

151 in ultrapure water (18.2 MΩ cm) to prepare an AS/Sucrose stock solution of 5 wt% at 1:1 molar

152 ratio. A 5-wt% aqueous solution of AS only and another of AS and SA (Sigma-Aldrich) mixed

153 at 1:1 weight ratio were also prepared. The prepared solution was atomized to produce droplets

154 using a piezoelectric particle generator (Model 201, Uni-Photon Inc.) and the analyte droplets

155 were deposited on a substrate of silicon wafer (100, N type, Y Mart, Inc.) that had been coated

156 with gold using a sputtering device (Q150T, Quorum Technologies Ltd.). The gold coating was

157 used to mask peaks of Si wafer at 520 and 900-1000 cm^{-1}. Ambient PM was collected on gold-

158 coated Si substrates at the South Gate of the Hong Kong University of Science and Technology

159 using a cascade impactor (Model MPS-4G1, California Measurements Inc.) on the morning of

160 9 May 2016. Collected particles between 0.05 and 0.15 µm in aerodynamic diameter were used

161 as analyte particles. The samples were kept in a desiccator at < 10% RH prior to use and Raman

162 measurements were taken at the ambient RH of 60%. All chemicals were used as received

163 without further purification.

164

165

2.2. SERS agent nanoparticles

167 Ag nanoparticles were deposited on the analyte particles (Fig. 1b) using the

168 electrospray technique (Gen and Lenggoro, 2015). An aqueous suspension of Ag nanoparticles

169 was prepared by reducing silver nitrate with sodium citrate (Lee and Meisel, 1982). The Ag

170 nanoparticles deposited on the substrate and in the suspension were characterized by scanning

171 electron microscopy (SEM; EVO 10, Carl Zeiss Inc. and JSM-6390, JEOL) and UV-vis

172 spectroscopy (UV-3600, Shimadzu), respectively. Ag nanoparticles suspended in the gas phase

173 produced from the electrospray were characterized with a differential mobility analyzer (DMA;

174 Model 3081A, TSI Inc.) and a condensation particle counter (CPC; Model 3025A, TSI Inc.).

175

2.3. Deposition of Ag nanoparticles

Figure 2 shows the electrospray system consisting of a generation and a deposition chamber. The suspension was diluted with an equal volume of ethanol to reduce the surface tension and to facilitate the evaporation of solvents (Gen and Lenggoro, 2015). The diluted suspension was fed to a stainless-steel capillary tube (SUS304; 32 gauge, Hamilton) which serves as a spray nozzle using a syringe pump (KDS-100, KD Scientific) at a liquid flow rate of 0.2 mL/h. The spray nozzle was inserted to a six-way cross chamber and positively charged at 2.0 - 2.5 kV with a high-voltage module (HV1, S1-5P(A)-L2, Matsusada Precision Inc.). The spray current, which is induced by charged droplets, was measured with an electrometer (Model 6485, Keithley Instruments Inc.). CO_2 gas at a flow rate of ~1 L/min was introduced into the chamber to suppress electric discharge (i.e. to maintain stability of electrospraying) (Zeleny, 1915) and carry Ag nanoparticles from the generation chamber to the deposition one. The spray nozzle and the deposition chamber were electrically separated from the generation chamber. The substrate was set perpendicular to the spray nozzle in the deposition chamber and negatively charged at - 2.0 kV using another high-voltage module (HV2, S1-5N(A)-L2, Matsusada Precision Inc.). Ag nanoparticles were deposited on the substrate at ambient pressure (1 atm) and the spraying time was 1 hour based on earlier work (Gen and Lenggoro, 2015). The Ag nanoparticles produced were electrically neutralized with a Kr-85 aerosol neutralizer (Model 3077A, TSI Inc.) before entering the DMA for size distribution measurements. Size classification in the DMA was performed by applying a negative voltage to the center rod of the DMA with a high-voltage supplier (HAR-15R2-L, Matsusada Precision Inc.). The voltage supplier was controlled with a data acquisition system (NI PCIe-6361, National Instruments) through a LabVIEW program using the necessary voltage for a specific

range of particle sizes based on the pressure and temperature of the flow in the DMA (Hinds, 1999; Knutson and Whitby, 1975).

2.4. SERS analysis

Analyte particles with and without Ag nanoparticles were characterized using a Raman spectroscope (Renishaw inVia Raman Microscope). Instrument control was performed with the Renishaw WiRE (Renishaw). Through microscopic observations, analyte particles exceeding 20 µm in diameter were selected for most cases of normal Raman and SERS measurements. A 633 nm (17 mW) laser was used and an integration time of 10 s was applied. The sample was irradiated with the laser through a 50X objective lens (N PLANEPI, $NA = 0.75$, Leica) and the laser spot size was estimated to be ~1 µm. Spectra from multiple positions on an analyte particle were acquired with a step size of 2 µm. Over 10 Raman spectra of 300-4000 cm^{-1} were obtained for each particle. Raman enhancement was observed for vibration modes of $v(SO_4^{2-})$, $v(NO_3^-)$, $v(C\text{-}H)$, and $v(O\text{-}H)$ at ~970, ~1034, ~2930 and 3200 ~ 3500 cm^{-1}, respectively. Ambient RH and temperature were 60% and 20-21 ℃, respectively. An enhancement factor is used to quantitatively examine the performance of SERS. This factor can be expressed as $(I_{SERS}/N_{Surf})/(I_{NR}/N_{vol})$, where N_{vol} is the average number of analyte molecules within the scattering volume for normal Raman experiments; N_{Surf} is the average number of analyte molecules physically and/or chemically adsorbed on a nanoparticle surface within the scattering volume for SERS experiments; I_{NR} and I_{SERS} are Raman intensities for normal Raman and SERS measurements, respectively (Le Ru et al., 2007). In the current study, we simply used I_{SERS}/I_{NR} for comparing experimental results later because it is difficult to calculate N_{vol}/N_{Surf}.

3. Results and discussion

We first characterize the electrospray technique. Next, SERS measurements of supermicron (1-40 µm) AS, AS/SA and AS/sucrose particles are reported. The presence of surface-adsorbed water is then discussed. Finally, ES-SERS is used to characterize submicron ambient PM. The SERS experimental results are shown in Table 1. More than 10 spectra for normal Raman and SERS measurements were quantified to estimate I_{SERS}/I_{NR}. All spectra for quantification of I_{SERS}/I_{NR} (except for AS /sucrose particles smaller than 20 µm) are shown in Figs. S1, S2 and S3.

3.1. Characterization of the electrospray system

The stability of the electrospraying system was characterized using the current (I)–voltage (V) curve (Figure S4 in the Supporting Information). Stable electrospraying can be obtained within a certain range of V where I does not change (de la Mora and Loscertales, 1994; Lenggoro et al., 2000). In Figure S4, I increases with V at lower V's (<2.0 kV). As V approaches 1.9 kV, I starts to level off and stays almost constant until V reaches 2.3 kV. In the present study, V ranged between 1.9 to 2.3 kV was used for electrospraying.

The dispersion of SERS nanoparticles and their interaction with analyte molecules determine the enhancement behavior (Ko et al., 2008; Oh et al., 2009; Addison and Brolo, 2006; Makiabadi et al., 2010; Sun et al., 2011). Therefore, Ag nanoparticles in the suspension, in the gas phase and deposited on the substrate were characterized. Figure S5 presents the absorption spectra of Ag nanoparticles in the suspension as prepared and as diluted with ethanol at a 1:1 volume ratio. The aqueous suspensions exhibited maximum absorption at ~ 400 nm as a result of the localized surface plasmon resonance, whereas the suspension diluted with

250   ethanol showed a slight shift to ~420 nm. This insignificant change in the absorption spectrum

251   suggests that the size distribution of Ag nanoparticles is similar before and after dilution. Figure

252   S6 shows the gas-phase size distribution of Ag nanoparticle aerosols with a mode of 53 nm in

253   electrical mobility diameter. The nanoparticles dried from the original suspension and those

254   deposited (electrosprayed) on the gold-coated silicon substrate were observed with SEM as

255   shown in Fig. S7 a and c, respectively. The size distribution of the deposited particles (Fig. S7

256   d) shows a peak of ~67 nm which is close to the primary particle size (56 nm in Fig. S7 b) and

257   the particle size (53 nm in Fig. S6) of the aerosol from the electrospray. The size of Ag

258   nanoparticles in suspension has been reported to be ~ 50 nm (Gen and Lenggoro, 2015). The

259   similarity in size between particles in the suspension, particles in the gas phase and particles

260   deposited on the substrate gives us confidence that the Ag nanoparticles produced in the current

261   system can be delivered from the suspension onto the substrate surface without much

262   aggregation.

263

264

265   **3.2. SERS of laboratory-generated PM**

266   Normal and enhanced Raman spectra of the AS/sucrose particles are shown in Fig. 3.

267   Normal Raman measurement of an AS/sucrose particle (without Ag nanoparticles) shows SO_4^{2-}

268   vibration modes at 450, 633, and 979 cm^{-1} and NH_4^+ vibration modes at 1461, 1700 and 3153

269   cm^{-1} (Dong et al., 2007). A broad band v(O-H) of water at ~3400 cm^{-1} can also be seen,

270   indicating that the particle contained bulk water at ambient RH (i.e. 60%). The addition of

271   sucrose delays efflorescence of the mixed particle (Chu and Chan, 2016). Bands v(C-O) of

272   sucrose at 1067 and 1130 cm^{-1} and a broad band v(C-H) at 2930 cm^{-1} were also observed

273   (Brizuela et al., 2014). In the presence of Ag nanoparticles, a significant Raman enhancement

274   was found at the v(SO_4^{2-}) mode of 967 cm^{-1} with I_{SERS}/I_{NR} = 12.4. The I_{SERS}/I_{NR} at v(SO_4^{2-})

275   mode is approximately 7.6 times higher than that at v(C-H) mode (Table 1). This is likely due

276   to the strong interaction between sulfate and Ag nanoparticles. Furthermore, a redshift from

277   980 to 967 cm^{-1} occurred. A commercially available Ag-coated SERS substrate (SERStrate,

278   Silmeco) (Schmidt et al., 2012) was also used to investigate the Raman enhancement of the

279   AS/sucrose particles (Fig. 4). Likewise, the selective enhancement and the redshift at the

280   v(SO$_4^{2-}$) mode were observed. In addition, the spectrum obtained with the SERS substrate

281   (green) is almost identical to the current SERS spectrum (red), giving us confidence that the

282   enhancement observed in the present study was triggered by the deposition of Ag nanoparticle

283   aerosols.

284   The electrospray system has been proven to be effective in depositing nanoparticles

285   onto any surface (Gen and Lenggoro, 2015). We believe that Ag nanoparticles are deposited

286   onto the analyte particle surfaces because Raman enhancement was observed only when

287   electrospraying Ag nanoparticles was performed. Ag nanoparticles used in the current study

288   were synthesized by the citrate-reduction method. If the nanoparticles were aggregated, SERS

289   spectrum would show enhanced peaks of citrate adsorbed on Ag nanoparticle surface as

290   stabilizer (Munro et al., 1995). In our measurements of AS particles, we observed strong citrate

291   peaks only for one particle (Figure S1(e)), but absent for all other SERS spectra. This gives us

292   confidence that the enhancement is mainly coming from individual Ag nanoparticles.

293   Strong charge-transfer interaction (i.e. chemisorption) between Ag nanoparticles and

294   analyte molecules generally leads to a peak shift and peak broadening (Campion and

295   Kambhampati, 1998; Stöckle et al., 2000). The strength of coupling is strongly dependent on

296   the orientation and binding of analyte molecules to a nanoparticle surface. Earlier work has

297   suggested that nitrate anions in aqueous form are chemisorbed on Ag nanoparticle surfaces,

298   resulting in a significant enhancement and a redshift of the v(NO$_3^-$) peak (Craig et al., 2015).

299   Similarly, aqueous sulfate is also expected to be chemisorbed on Ag nanoparticles, leading to

300   a significant enhancement of the $v(SO_4^{2-})$ peak. In other words, the availability of aqueous

301   sulfate on the surface of analyte particles, $[SO_4^{2-}]$ could be characterized by the enhancement.

302   To study the Raman enhancement of $[SO_4^{2-}]$, SERS was performed on the AS and AS/SA

303   particles. The sample particles were first dried at below 10% RH and then exposed to 60% RH

304   during the normal Raman and SERS measurements. Both types of particles are in solid form

305   at 60% RH (Laskina et al., 2015; Choi and Chan, 2002). There is no difference in the full width

306   at half maximum (FWHM) and the peak position between AS and AS/SA particles (see Table

307   2), confirming that the presence of SA does not affect the phase state of AS at 60% RH. Figure

308   5 shows the normal and SERS spectra of the AS and AS/SA particles. No Raman enhancement

309   at the $v(SO_4^{2-})$ mode was observed for the AS particles (i.e. $I_{SERS}/I_{NR} \sim 1$). Since the AS

310   particles were solid during SERS measurements, a negligible amount of aqueous sulfate anions

311   were available. In contrast, the AS/SA particles show an enhancement at $\delta(OH \cdots O)$, $v(SO_4^{2-})$

312   and $v(C\text{-}H)$ modes with the I_{SERS}/I_{NR} of 3.7, 3.3 and 2.6, respectively. The I_{SERS}/I_{NR} at the

313     $v(SO_4^{2-})$ mode is significantly smaller than $I_{SERS}/I_{NR} = 12.4$ for the AS/sucrose particles,

314   suggesting that less surface aqueous sulfate for the AS/SA particles was available than that for

315   the AS/sucrose particles. SA, which is only slightly soluble in water, crystallizes and forms

316   nuclei during the partial efflorescence of ammonium nitrate and AS (Lightstone et al., 2000).

317   The presence of SA does not affect the deliquescence behavior of AS (Choi and Chan, 2002).

318   Nonetheless, the current results clearly demonstrate that the addition of SA into AS has a

319   substantial influence on the availability of aqueous sulfate anions on the analyte particle surface

320   but not so much on their availability in the AS particle system. Overall, SERS experiments

321   reveal the availability of surface aqueous sulfate in the three particle systems: $[SO_4^{2-}]_{AS/sucrose}$

322     $(I_{SERS}/I_{NR} = 12.4) > [SO_4^{2-}]_{AS/SA}$ $(I_{SERS}/I_{NR} = 3.3) > [SO_4^{2-}]_{AS}$ $(I_{SERS}/I_{NR} = 1)$.

323   Particle phase can be inferred from the position and shape of the Raman peaks (Yeung

324   and Chan, 2010). Table 2 shows the peak position and FWHM of the $v(SO_4^{2-})$ mode obtained

325 using Gaussian fittings. When AS deliquesces, the $v(SO_4^{2-})$ peak is generally blue-shifted and

326 broadened. In the normal Raman measurements, AS and AS/SA particles show a sharp peak at

327 977 cm^{-1} with FWHM of <8 cm^{-1} but the AS/sucrose particles show a peak at 980 cm^{-1} with

328 FWHM of 13.5 cm^{-1}. The blueshift and band broadening strongly suggest the presence of

329 aqueous sulfate in the AS/sucrose particles, whereas the other particles contain sulfate in solid

330 form. In the SERS measurements, however, the redshift and increase in FWHM are most likely

331 due to strong interaction between Ag nanoparticles and surface aqueous sulfate (Niaura and

332 Malinauskas, 1998). The shape of the $v(SO_4^{2-})$ peak for the AS particles did not change between

333 the two measurements, indicating no or weak interaction between Ag nanoparticles and sulfate

334 in solid form.

335    Figure 6 shows Raman intensities at the $v(SO_4^{2-})$ mode along the diameter of individual

336 AS/sucrose particles from normal Raman and SERS measurements. The laser spot transected

337 the particle surface from one edge to another edge with a step size of 2 µm. Normal Raman

338 measurement showed peaks of the $v(SO_4^{2-})$ mode at all positions. SERS measurement showed

339 an enhancement at all positions, although the Raman intensity fluctuated. The results

340 demonstrate the high-frequency Raman enhancement across an individual particle. The higher

341 SERS intensities near the edges might be due to the higher densities of SERS active spots in

342 the sensing volume of the laser spot.

343

344

345 **3.3. Size effect on Raman intensity**

346    One of the essential requirements for Raman enhancement is that analyte molecules

347 must be located within a few nanometers of the nanoparticle surface (Dieringer et al., 2006).

348 Raman emissions from analyte molecules far from the surface cannot be enhanced. Hence, the

349 enhanced Raman spectra can provide chemical information about the surface of analyte

350 particles. Here we examine the effect of analyte particle size (i.e. particle volume) on Raman

351 signals to confirm the surface-sensitive Raman emissions. Figure 7 shows the typical normal

352 Raman spectrum of AS/sucrose particles and the intensities of $v(SO_4^{2-})$ and $v(C-H)$ as a

353 function of the particle size. Small particles were produced using stock solutions of AS/sucrose

354 diluted by a factor of 10 and 100. Above 10 µm in particle size, the Raman intensity stays

355 almost constant for both modes. When the particle size is below 10 µm, the Raman intensity

356 decreases with particle size. Raman intensity is correlated with the number of analyte

357 molecules in the sensing volume of the focused laser spot. The size dependence indicates that

358 normal Raman measurements are sensitive to the particle volume and provides bulk

359 information about the chemical composition of analyte particles. Note that the laser spot size

360 is smaller than any of the particle size studied and therefore particle width has no effect on the

361 intensity. However, the depth of focus, h, contributes to the size effect on the intensity. If the

362 analyte particle depth is comparable to or smaller than h, the Raman intensity decreases with

363 the number of molecules within the sensing volume. The estimated h in our experiments is 2.3

364 µm using $h = 2\lambda/NA^2$ where λ (633 nm) and NA (0.75) are the wavelength of the laser and the

365 numerical aperture of the objective lens, respectively. This estimated value is smaller than the

366 nominal threshold of 10 µm observed in the size dependence of the normal Raman signals,

367 because gravity had affected the shape of the analyte particles deposited on the substrate,

368 reducing the particle height (<10 µm). Gravity deforms the shape of droplets on a substrate,

369 when the size of droplet is sufficiently large (e.g. > 10 µm). A contact angle of large droplet to

370 a substrate is much smaller than 180 degrees. Thus, the depth of substrate-deposited droplet is

371 typically smaller than its diameter. Earlier work using environmental SEM has shown that AS

372 droplets are hemispherical when in contact at 96º with a copper substrate that has been

373 hydrophobically modified with poly-tetrafluoroethylene (Matsumura and Hayashi, 2007).

374   Figure 8 shows the typical enhanced spectra of the AS/sucrose and the intensity as a

375   function of particle size for the two modes. Unlike the normal Raman measurements, the

376   enhanced intensity as a function of particle size was almost constant. SERS active spots were

377   created over the surface of analyte particles and the surface area irradiated by a laser was

378   constant over the size range studied due to the smaller laser spot diameter. Furthermore, in the

379   normal Raman measurements, a change in particle size changes the Raman intensity when the

380   particle volume is comparable to the sensing volume of the laser spot. Considering these facts,

381   the constant enhanced intensity provides evidence that the enhanced spectrum contains

382   information about the bulk chemical compositions (non-enhanced component) as well as the

383   surface compositions (enhanced component), making the ES-SERS technique suitable for

384   surface-sensitive detection.

385   The I_{SERS}/I_{NR} ratio as a function of particle size for the AS/sucrose particles is

386   summarized in Table 1. I_{SERS} was calculated by averaging enhanced peak intensities from all

387   SERS measurements (the entire size range). The normal Raman intensity decreases with size

388   below 10 µm. Hence I_{SERS}/I_{NR} increases with decreasing size, resulting in the largest I_{SERS}/I_{NR}

389   of 162.0 for the $v(SO_4^{2-})$ mode at a particle size of 1.4 µm. Craig et al. (2015) reported an

390   enhancement factor of 2.0 at $v(SO_4^{2-})$ mode of ~970 cm^{-1} using an SERS substrate with the AS

391   particles on the top of Ag nanoparticles on the substrate. Furthermore, Fu et al. (2017) reported

392   an enhancement factor of 6.1 for the same mode, using commercial SERS substrates with pre-

393   determined gold-coated structure of inverted pyramids (Klarite, Renishaw Diagnostics Ltd.).

394   Our results of AS/sucrose particles (Table 1) showed that the I_{SERS}/I_{NR}, which is the lower limit

395   of enhancement factor, ranged from 12.4 to 163, much higher than the above studies. Note that

396   I_{SERS}/I_{NR} is the lower limit of the enhancement factor ($I_{SERS}N_{vol}/I_{NR}N_{surf}$) conventionally used

397   because N_{vol}/N_{surf} is much greater than unity in the present case.

398

399

3.4. Measurements of surface-adsorbed water

Taking advantage of the surface sensitiveness of ES-SERS, we examine the presence of surface-adsorbed water on solid particles of AS and AS/SA. As shown in Fig. 3 and Table 2, AS/sucrose particles (1:1 molar ratio) at 60% RH are aqueous, which can be inferred from the blueshift in the $v(SO_4^{2-})$ peak compared to the AS particles, a broad peak at the $v(C-H)$ mode and the appearance of the $v(O-H)$ mode of water (~3400 cm^{-1}). The enhancement at the $v(O-H)$ mode (I_{SERS}/I_{NR} = 1.2) was observed in the AS/sucrose particles, but bulk water might have contributed to the enhancement. Figure 9 presents the normal and enhanced Raman spectra of solid AS and AS/SA particles at 3000 ~ 4000 cm^{-1} at 60% RH, and reveals a possible role of surface-adsorbed water formed on the particles. No water peak was observed at $v(O-H)$ in the normal Raman measurements of either particle system (blue spectra) confirming that the particle phases were likely solid and the bulk water in the particles was negligible (undetectable). In contrast, the SERS experiments presented a slightly enhanced water peak for the AS particles and a significant enhancement for the AS/SA particles. The thickness of surface-adsorbed water on AS at 60% has been reported to be ~ 0.19 nm (a monolayer) (Romakkaniemi et al., 2001). The slight enhancement reflects the detection limit in our approach (i.e. a water film of monolayer thickness). The significant enhancement for AS/SA particles, which was much larger than that for AS particles, suggests that they had more than one layer of adsorbed water at 60% RH. The presence of water at 60% RH could explain the gradual mass increase of AS/SA particles before abrupt water uptake at deliquescence (Ling and Chan, 2008). The relative mass change (m/m_0) obtained with an electrodynamic balance increases with RH: m/m_0 = 1.0, 1.2, 1.3 and 2.0 at 50%, 80%, 81% and 82% RH, respectively. Corresponding Raman spectra did not show a distinct peak at $v(O-H)$ mode at RHs between 50 and 81%.

424   The surface-adsorbed water may have facilitated the dissolution of sulfate anions into

425 its layer(s) from the bulk particle, thus contributing to an increase in aqueous sulfate anions on

426 the surface (Fig. 9c). In other words, the surface-adsorbed water is likely associated with the

427 aqueous sulfate anions on the surface, which is consistent with our observation on the

428 availability of aqueous sulfate anions for the AS and AS/SA particles ($[SO_4^{2-}]_{AS/SA} > [SO_4^{2-}]_{AS}$).

429 Sulfate in the bulk solid phase dissolved in the surface-adsorbed water layer(s) and was

430 subsequently chemisorbed on the surface of an Ag nanoparticle, leading to a significant Raman

431 enhancement and a peak shift.

432

433

434 **3.5. Ambient PM**

435   Lastly, we present SERS experiments of ambient PM. Figure 10 shows the normal and

436 enhanced Raman spectra of the ambient PM and the conceptual representations of the analyte

437 particles for normal Raman and SERS measurements. The normal spectrum has peak bands of

438 SO_4^{2-} vibration at 451, 615 and 977 cm^{-1} as well as disorder (D) and graphite (G) peak bands

439 at 1341 and 1598 cm^{-1} respectively. The presence of D and G bands reveals that the particles

440 contain non-graphite and graphite components, which are often referred to as amorphous

441 carbon or black carbon (BC) (Sze et al., 2001). The SERS experiments show a small

442 enhancement at bands of 963 cm^{-1} (I_{SERS}/I_{NR} = 1.9) for sulfate and 1039 cm^{-1} (I_{SERS}/I_{NR} = 1.6)

443 for nitrate, but no enhancement of the D and G peaks. I_{SERS}/I_{NR} was quantified from the

444 measurements from 43 different positions on the substrate. A water peak band was not found

445 at ~3400 cm^{-1} (not shown), suggesting that the bulk water was negligible. Nonetheless, the

446 small enhancement at 963 cm^{-1} indicates the presence of surface-adsorbed water on ambient

447 PM at 60% RH, which helps sulfate dissolve in the water layer(s). A peak shift from 977 to

448 963 cm^{-1} and an increase in FWHM from 7.6 to 26.0 cm^{-1} indicate that sulfate anions were

449   chemisorbed on the Ag particle surface (Fig. 9c). Additionally, the enhanced spectrum presents

450   a peak band at 1777 cm^{-1}, which can be assigned to the carbonyl group. A similar observation

451   using normal Raman spectroscopy has been reported for particles collected in Hamilton,

452   Ontario (Sze et al., 2001). The PM probably contained organics, but the amount of organics

453   could not be detected in mass in the normal Raman measurements. Overall, the normal Raman

454   spectra represent the bulk chemical compositions of BC and sulfate. The enhanced spectra

455   exhibit the bulk chemical compositions together with the surface compositions (e.g. sulfate and

456   the carbonyl group). On the basis of the selective enhancement of the sulfate peak and to a

457   lesser extent the carbonyl peak, we postulate that these BC particles may have been coated with

458   organics and sulfate. In the atmosphere, BC aerosols are usually internally mixed with organics

459   and sulfate after aging (Shiraiwa et al., 2007). An integrated approach using Raman

460   spectroscopy and sum frequency generation spectroscopy has shown that organic material

461   primarily exists at the gas/particle interface of sea spray aerosols (Ault et al., 2013). The

462   spectrum obtained from ES-SERS contains both bulk and surface information of chemical

463   compositions, but only the surface compositions are enhanced due to the distance-dependence

464   effect (Dieringer et al., 2006). The complementary methods of Raman spectroscopy and ES-

465   SERS (as surface-sensitive spectroscopy) can provide the bulk and surface chemical

466   compositions, respectively by comparing normal and enhanced Raman spectra. They

467   potentially help reveal the internal structure of individual particles such as their core/shell

468   structure.

469

470

471   **4. Conclusions**

472   We demonstrated a new technique called ES-SERS for probing atmospherically relevant

473   particle compositions. ES-SERS measurements showed that the I_{SERS}/I_{NR} ratios of the $v(SO_4^{2-})$

474 band at ~970 cm^{-1} for laboratory-generated AS, AS/SA and AS/sucrose particles followed the

475 order: AS/sucrose (I_{SERS}/I_{NR} = 12.4) > AS/SA (I_{SERS}/I_{NR} = 3.3) > AS (I_{SERS}/I_{NR} = 1). I_{SERS}/I_{NR}

476 is likely associated with the availability of aqueous sulfate anions on the surface, which can be

477 characterized by the enhanced Raman signals, the redshift and the increase in FWHM due to

478 the chemisorption of aqueous sulfate anions on Ag nanoparticles.

479   The ES-SERS technique also allows us to probe the presence of surface-adsorbed water.

480 At 60% RH, the normal Raman spectra of solid AS and AS/SA particles do not exhibit a peak

481 band of v(O-H) at ~3400 cm^{-1} but the enhanced spectra show a small enhancement for AS

482 particles and a significant enhancement for AS/SA particles. The latter is attributable to water

483 adsorbed on the surface of the solid particles. The surface-adsorbed water may promote the

484 dissolution of sulfate from the bulk phase into its water layer(s). The enhanced v(SO$_4^{2-}$) peaks

485 also revealed that the AS/SA particles have more surface aqueous sulfate than do the AS

486 particles.

487   While the normal Raman intensity was sensitive to the particle size, the enhanced

488 Raman intensity was insensitive in the size range studied (1 ~ 40 µm). In fact, the enhanced

489 intensity was constant over the entire size range. Increasing attention has been paid to

490 spectroscopic analysis which can provide valuable information on the physicochemical

491 properties of atmospheric particles at the single-particle level (Ciobanu et al., 2009; Baustian

492 et al., 2012; Yeung et al., 2009). One of the biggest limitations is that particles must be at least

493 1 µm in size for particle analysis to be possible due to the Abbe diffraction limit. Our ES-SERS

494 results demonstrate that the enhanced Raman signals do not drop as the particle size decreases

495 down to 2 µm. The high sensitivity is likely due to the configuration of the SERS active spots.

496 This sensitive technique may be extended to submicron particles in future studies.

497   Normal spectra of ambient submicron PM show the D and G bands and the v(SO$_4^{2-}$)

498 band, revealing that the particles contain amorphous carbon (i.e. BC) and sulfate. The enhanced

spectra exhibit selective enhancement of $v(SO_4^{2-})$ and $v(C=O)$ modes but no enhancement for the D and G bands. Based on a comparison of the spectra, we postulate a particle morphology with sulfate and organics surrounding the BC core.

The direct contact of Ag nanoparticles to analyte molecules results in a peak shift, which could pose an obstacle to tracing the phase transition as well as identifying functional groups. Recent studies have introduced the use of core-shell composite gold nanoparticles to eliminate the chemical enhancement (Li et al., 2010; Li et al., 2013). The outermost inert shell layer of the nanoparticle prevents its direct contact (i.e. coupling) with analyte molecules. Using such novel nanoparticles could further extend the application of the proposed ES-SERS technique in atmospheric studies.

Acknowledgements

The authors would like to acknowledge Prof. Chun Sing Lee and Dr. Zhi Ning of City University of Hong Kong for the use of their Raman spectrometer and condensation particle counter respectively. The authors also would like to acknowledge Hong Kong University of Science and Technology for the use of their scanning electron microscope (JSM-6390, JEOL).

524

525

526

527

528

529

530

531

532

533

534

References

Addison, C. J., and Brolo, A. G.: Nanoparticle-containing structures as a substrate for surface-enhanced Raman scattering, Langmuir, 22, 8696-8702, doi: 10.1021/la061598c, 2006.

Albrecht, M. G., and Creighton, J. A.: Anomalously intense Raman-spectra of pyridine at a silver electrode, J. Am. Chem. Soc., 99, 5215-5217, doi: 10.1021/ja00457a071, 1977.

Ault, A. P., and Axson, J. L.: Atmospheric aerosol chemistry: spectroscopic and microscopic advances, Anal. Chem., 89, 430-452, doi: 10.1021/acs.analchem.6b04670, 2017.

Ault, A. P., Zhao, D., Ebben, C. J., Tauber, M. J., Geiger, F. M., Prather, K. A., and Grassian, V. H.: Raman microspectroscopy and vibrational sum frequency generation spectroscopy as probes of the bulk and surface compositions of size-resolved sea spray aerosol particles, Phys. Chem. Chem. Phys., 15, 6206-6214, doi: 10.1039/c3cp43899f, 2013.

Baustian, K. J., Cziczo, D. J., Wise, M. E., Pratt, K. A., Kulkarni, G., Hallar, A. G., and Tolbert, M. A.: Importance of aerosol composition, mixing state, and morphology for

549 heterogeneous ice nucleation: A combined field and laboratory approach, J. Geophys.

550 Res., 117, D06217, doi: 10.1029/2011jd016784, 2012.

551 Bertram, A. K., Martin, S. T., Hanna, S. J., Smith, M. L., Bodsworth, A., Chen, Q., Kuwata,

552 M., Liu, A., You, Y., and Zorn, S. R.: Predicting the relative humidities of liquid-liquid

553 phase separation, efflorescence, and deliquescence of mixed particles of ammonium

554 sulfate, organic material, and water using the organic-to-sulfate mass ratio of the

555 particle and the oxygen-to-carbon elemental ratio of the organic component, Atmos.

556 Chem. Phys., 11, 10995-11006, doi: 10.5194/acp-11-10995-2011, 2011.

557 Brizuela, A. B., Castillo, M. V., Raschi, A. B., Davies, L., Romano, E., and Brandán, S. A.: A

558 complete assignment of the vibrational spectra of sucrose in aqueous medium based on

559 the SQM methodology and SCRF calculations, Carbohydr. Res., 388, 112-124, doi:

560 10.1016/j.carres.2013.12.011, 2014.

561 Campion, A., and Kambhampati, P.: Surface-enhanced Raman scattering, Chem. Soc. Rev., 27,

562 241-250, doi: 10.1039/a827241z, 1998.

563 Choi, M. Y., and Chan, C. K.: The effects of organic species on the hygroscopic behaviors of

564 inorganic aerosols, Environ. Sci. Technol., 36, 2422-2428, doi: 10.1021/es0113293,

565 2002.

566 Chu, Y., and Chan, C. K.: Reactive uptake of dimethylamine by ammonium sulfate and

567 ammonium sulfate–sucrose mixed particles, J. Phys. Chem. A, 121, 206–215, doi:

568 10.1021/acs.jpca.6b10692, 2016.

569 Ciobanu, V. G., Marcolli, C., Krieger, U. K., Weers, U., and Peter, T.: Liquid-liquid phase

570 separation in mixed organic/inorganic aerosol particles, J. Phys. Chem. A, 113, 10966-

571 10978, doi: 10.1021/jp905054d, 2009.

572 Craig, R. L., Bondy, A. L., and Ault, A. P.: Surface enhanced Raman spectroscopy enables

573 observations of previously undetectable secondary organic aerosol components at the

574   individual   particle   level,   Anal.   Chem.,   87,   7510-7514,   doi:

575   10.1021/acs.analchem.5b01507, 2015.

576 de la Mora, J. F.: The fluid dynamics of Taylor cones, Annu. Rev. Fluid Mech., 39, 217-243,

577   doi: 10.1146/annurev.fluid.39.050905.110159, 2007.

578 de la Mora, J. F., and Loscertales, I. G.: The current emitted by highly conducting Taylor cones,

579   J. Fluid Mech., 260, 155-184, doi: 10.1017/s0022112094003472, 1994.

580 DeMott, P. J., Hill, T. C. J., McCluskey, C. S., Prather, K. A., Collins, D. B., Sullivan, R. C.,

581   Ruppel, M. J., Mason, R. H., Irish, V. E., Lee, T., Hwang, C. Y., Rhee, T. S., Snider, J.

582   R., McMeeking, G. R., Dhaniyala, S., Lewis, E. R., Wentzell, J. J. B., Abbatt, J., Lee,

583   C., Sultana, C. M., Ault, A. P., Axson, J. L., Martinez, M. D., Venero, I., Santos-

584   Figueroa, G., Stokes, M. D., Deane, G. B., Mayol-Bracero, O. L., Grassian, V. H.,

585   Bertram, T. H., Bertram, A. K., Moffett, B. F., and Franc, G. D.: Sea spray aerosol as

586   a unique source of ice nucleating particles, Proc. Natl. Acad. Sci. U.S.A., 113, 5797-

587   5803, doi: 10.1073/pnas.1514034112, 2016.

588 Dieringer, J. A, McFarland, A. D., Shah, N. C., Stuart, D. A., Whitney, A. V., Yonzon, C. R.,

589   Young, M. A., Zhang, X., and Van Duyne, R. P.: Surface enhanced Raman

590   spectroscopy: new materials, concepts, characterization tools, and applications, Farad.

591   Discuss., 132, 9-26, doi: 10.1039/B513431P, 2006.

592 Dong, J. L., Li, X. H., Zhao, L. J., Xiao, H. S., Wang, F., Guo, X., and Zhang, Y. H.: Raman

593   observation of the interactions between NH_4^+, SO_4^{2-}, and H_2O in supersaturated

594          $(NH_4)_2SO_4$ droplets, J. Phys. Chem. B, 111, 12170-12176, doi: 10.1021/jp072772o,

595   2007.

596 Ewing, G. E.: Ambient thin film water on insulator surfaces, Chem. Rev., 106, 1511-1526, doi:

597   10.1021/cr040369x, 2006.

598   Freedman, M. A., Baustian, K. J., Wise, M. E., and Tolbert, M. A.: Characterizing the

599   morphology of organic aerosols at ambient temperature and pressure. Anal. Chem., 82,

600   7965-7972, doi: 10.1021/ac101437w, 2010.

601   Fu, Y., Kuppe, C., Valev, V. K., Fu, H., Zhang, L., and Chen, J.: Surface-enhanced Raman

602   spectroscopy: A facile and rapid method for the chemical component study of

603   individual atmospheric aerosol, Environ. Sci. Technol, 51, 6260-6267, doi:

604   10.1021/acs.est.6b05910, 2017.

605   Gen, M., and Lenggoro, I. W.: Probing a dip-coated layer of organic molecules by an aerosol

606   nanoparticle sensor with sub-100 nm resolution based on surface-enhanced Raman

607   scattering, RSC Adv., 5, 5158-5163, doi: 10.1039/c4ra03850a, 2015.

608   Hinds, W. C.: Aerosol Technology: Properties, Behavior, and Measurement of Airborne

609   Particles, New York, Wiley, 1999.

610   IPCC: Climate Change 2013: The Physical Science Basis: Summary for Policymakers,

611   Cambridge, UK, 2013.

612   Jaworek, A.: Micro- and nanoparticle production by electrospraying, Powder Technol., 176,

613   18-35, doi: 10.1016/j.powtec.2007.01.035, 2007.

614   Jeanmaire, D. L., and Van Duyne, R. P.: Surface raman spectroelectrochemistry: Part I.

615   Heterocyclic, aromatic, and aliphatic amines adsorbed on the anodized silver electrode,

616   J. Electroanal. Chem., 84, 1-20, doi: 10.1016/s0022-0728(77)80224-6, 1977.

617   Kim, H., Kim, J., Yang, H., Suh, J., Kim, T., Han, B., Kim, S., Kim, D. S., Pikhitsa, P. V., and

618   Choi, M.: Parallel patterning of nanoparticles via electrodynamic focusing of charged

619   aerosols, Nat. Nanotechnol., 1, 117-121, doi: 10.1038/nnano.2006.94, 2006.

620   Knutson, E. O., and Whitby, K. T.: Aerosol classification by electric mobility: apparatus,

621   theory, and applications, J. Aerosol Sci., 6, 443-451, doi: 10.1016/0021-8502(75)

622   90060-9, 1975.

623 Ko, H., Singamaneni, S., and Tsukruk, V. V.: Nanostructured surfaces and assemblies as SERS

624   media, Small, 4, 1576-1599, doi: 10.1002/smll.200800337, 2008.

625 Laskina, O., Morris, H. S., Grandquist, J. R., Qiu, Z., Stone, E. A., Tivanski, A. V., and

626   Grassian, V. H.: Size matters in the water uptake and hygroscopic growth of

627   atmospherically relevant multicomponent aerosol particles, J. Phys. Chem. A, 119,

628   4489-4497, doi: 10.1021/jp510268p, 2015.

629 Le Ru, E. C., Blackie, E., Meyer, M., and Etchegoin, P. G.: Surface enhanced Raman scattering

630   enhancement factors: A comprehensive study, J. Phys. Chem. C, 111, 13794-13803,

631   doi: 10.1021/jp0687908, 2007.

632 Lee, A. K. Y., and Chan, C. K.: Heterogeneous reactions of linoleic acid and linolenic acid

633   particles with ozone: Reaction pathways and changes in particle mass, hygroscopicity,

634   and morphology, J. Phys. Chem. A, 111, 6285-6295, doi: 10.1021/jp071812l, 2007.

635 Lee, P. C., and Meisel, D.: Adsorption and surface-enhanced Raman of dyes on silver and gold

636   sols, J. Phys. Chem., 86, 3391-3395, doi: 10.1021/j100214a025, 1982.

637 Lenggoro, I. W., Lee, H. M., and Okuyama, K.: Nanoparticle assembly on patterned

638   "plus/minus" surfaces from electrospray of colloidal dispersion, J. Colloid Interface

639   Sci., 303, 124-130, doi: 10.1016/j.jcis.2006.07.033, 2006.

640 Lenggoro, I. W., Okuyama, K., de la Mora, J. F., and Tohge, N.: Preparation of ZnS

641   nanoparticles by electrospray pyrolysis, J. Aerosol Sci., 31, 121-136, doi:

642   10.1016/s0021-8502(99)00534-0, 2000.

643 Li, J. F., Huang, Y. F., Ding, Y., Yang, Z. L., Li, S. B., Zhou, X. S., Fan, F. R., Zhang, W.,

644   Zhou, Z. Y., Wu, D. Y., Ren, B., Wang, Z. L., and Tian, Z. Q.: Shell-isolated

645   nanoparticle-enhanced Raman spectroscopy, Nature, 464, 392-395, doi:

646   10.1038/nature08907, 2010.

647 Li, J. F., Tian, X. D., Li, S. B., Anema, J. R., Yang, Z. L., Ding, Y., Wu, Y. F., Zeng, Y. M.,

648 Chen, Q. Z., Ren, B., Wang, Z. L., and Tian, Z. Q.: Surface analysis using shell-isolated

649 nanoparticle-enhanced Raman spectroscopy, Nat. Protoc., 8, 52-65, doi:

650 10.1038/nprot.2012.141, 2013.

651 Lightstone, J. M., Onasch, T. B., Imre, D., and Oatis, S.: Deliquescence, efflorescence, and

652 water activity in ammonium nitrate and mixed ammonium nitrate/succinic acid

653 microparticles, J. Phys. Chem. A, 104, 9337-9346, doi: 10.1021/jp002137h, 2000.

654 Ling, T. Y., and Chan, C. K.: Partial crystallization and deliquescence of particles containing

655 ammonium sulfate and dicarboxylic acids, J. Geophys. Res., 113, D14205, doi:

656 10.1029/2008jd009779, 2008.

657 Makiabadi, T., Bouvrée, A., Le Nader, V., Terrisse, H., and Louarn, G.: Preparation,

658 optimization, and characterization of SERS sensor substrates based on two-dimensional

659 structures of gold colloid, Plasmonics, 5, 21-29, doi: 10.1007/s11468-009-9110-6, 2010.

660 Matsumura, T., and Hayashi, M.: Hygroscopic growth of an $(NH_4)_2SO_4$ aqueous solution

661 droplet measured using an environmental scanning electron microscope (ESEM),

662 Aerosol Sci. Technol., 41, 770-774, doi: 10.1080/02786820701436831, 2007.

663 Munro, C. H., Smith, W. E., Garner, M., Clarkson, J. W. P. C., and White, P. C.:

664 Characterization of the surface of a citrate-reduced colloid optimized for use as a

665 substrate for surface-enhanced resonance Raman scattering, Langmuir, 11, 3712-3720,

666 doi: 10.1021/la00010a021, 1995.

667 Niaura, G., and Malinauskas, A.: Surface-enhanced Raman spectroscopy of ClO_4^- and SO_4^{2-}

668 anions adsorbed at a Cu electrode, J. Chem. Soc. Faraday Trans., 94, 2205-2211, doi:

669 10.1039/a800574e, 1998.

670   Ofner, J., Deckert-Gaudig, T., Kamilli, K. A., Held, A., Lohninger, H., Deckert, V., and Lendl,

671   B.: Tip-enhanced Raman spectroscopy of atmospherically relevant aerosol

672   nanoparticles, Anal. Chem., 88, 9766-9772, doi: 10.1021/acs.analchem.6b02760, 2016.

673   Oh, M. K., Yun, S., Kim, S. K., and Park, S.: Effect of layer structures of gold nanoparticle

674   films on surface enhanced Raman scattering, Anal. Chim. Acta, 649, 111-116, doi:

675   10.1016/j.aca.2009.07.025, 2009.

676   Okuyama, K., and Lenggoro, I. W.: Preparation of nanoparticles via spray route, Chem. Eng.

677   Sci., 58, 537-547, doi: 10.1016/s0009-2509(02)00578-x, 2003.

678   Pope, C. A., and Dockery, D. W.: Health effects of fine particulate air pollution: Lines that

679   connect, J. Air & Waste Manage. Assoc., 56, 709-742, doi:

680   10.1080/10473289.2006.10464485, 2006.

681   Romakkaniemi, S., Hämeri, K., Väkevä, M., and Laaksonen, A.: Adsorption of water on 8− 15

682   nm NaCl and $(NH_4)_2SO_4$ aerosols measured using an ultrafine tandem differential

683   mobility analyzer, J. Phys. Chem. A, 105, 8183-8188, doi: 10.1021/jp010647l, 2001.

684   Schmidt, M. S., Hübner, J., and Boisen, A.: Large area fabrication of leaning silicon nanopillars

685   for surface enhanced Raman spectroscopy, Adv. Mater., 24, OP11-OP18, doi:

686   10.1002/adma.201103496, 2012.

687   Shiraiwa, M., Kondo, Y., Moteki, N., Takegawa, N., Miyazaki, Y., and Blake, D. R.: Evolution

688   of mixing state of black carbon in polluted air from Tokyo, Geophys. Res. Lett., 34,

689   L16803, doi: 10.1029/2007GL029819, 2007.

690   Sobanska, S., Hwang, H., Choël, M., Jung, H. J., Eom, H. J., Kim, H., Barbillat, J., and Ro, C.

691   U.: Investigation of the chemical mixing state of individual asian dust particles by the

692   combined use of electron probe X-ray microanalysis and Raman microspectrometry,

693   Anal. Chem., 84, 3145-3154, doi: 10.1021/ac2029584, 2012.

694 Stöckle, R. M., Suh, Y. D., Deckert, V., and Zenobi, R.: Nanoscale chemical analysis by tip-
695   enhanced Raman spectroscopy, Chem. Phys. Lett., 318, 131-136, doi: 10.1016/s0009-
696   2614(99)01451-7, 2000.

697 Sullivan, R. C., and Prather, K. A.: Recent advances in our understanding of atmospheric
698   chemistry and climate made possible by on-line aerosol analysis instrumentation, Anal.
699   Chem., 77, 3861-3886, doi: 10.1021/ac050716i, 2005.

700 Sun, L., Zhao, D., Ding, M., Xu, Z., Zhang, Z., Li, B., and Shen, D.: Controllable synthesis of
701   silver nanoparticle aggregates for surface-enhanced Raman scattering studies, J. Phys.
702   Chem. C, 115, 16295-16304, doi: 10.1021/jp205545g, 2011.

703 Sze, S.-K., Siddique, N., Sloan, J. J., and Escribano, R.: Raman spectroscopic characterization
704   of carbonaceous aerosols, Atmos. Environ., 35, 561-568, doi: 10.1016/S1352-
705   2310(00)00325-3, 2001.

706 Trainic, M., Riziq, A. A., Lavi, A., and Rudich, Y.: Role of interfacial water in the
707   heterogeneous uptake of glyoxal by mixed glycine and ammonium sulfate aerosols, J.
708   Phys. Chem. A, 116, 5948-5957, doi: 10.1021/jp2104837, 2012.

709 Uzayisenga, V., Lin, X.-D., Li, L.-M., Anema, J. R., Yang, Z.-L., Huang, Y.-F., Lin, H.-X., Li,
710   S.-B., Li, J.-F., and Tian, Z.-Q.: Synthesis, characterization, and 3D-FDTD simulation
711   of Ag@ SiO_2 nanoparticles for shell-isolated nanoparticle-enhanced Raman
712   spectroscopy, Langmuir, 28, 9140-9146, doi: 10.1021/la3005536, 2012.

713 Yang, Z., Aizpurua, J., and Xu, H.: Electromagnetic field enhancement in TERS configurations,
714   J. Raman Spectrosc., 40, 1343-1348, doi: 10.1002/jrs.2429, 2009.

715 Yeung, M. C., and Chan, C. K.: Water content and phase transitions in particles of inorganic
716   and organic species and their mixtures using micro-Raman spectroscopy, Aerosol Sci.
717   Technol., 44, 269-280, doi: 10.1080/02786820903583786, 2010.

718   Yeung, M. C., Lee, A. K. Y., and Chan, C. K.: Phase transition and hygroscopic properties of

719   internally mixed ammonium sulfate and adipic acid (AS-AA) particles by optical

720   microscopic imaging and Raman spectroscopy, Aerosol Sci. Technol., 43, 387-399,

721   doi: 10.1080/02786820802672904, 2009.

722   Zeleny, J.: On the conditions of instability of electrified drops, with applications to the

723   electrical discharge from liquid points, Proc. Cambridge Philos. Soc., 18, 71-83, 1915.

724   Zobrist, B., Marcolli, C., Pedernera, D. A., and Koop, T.: Do atmospheric aerosols form

725   glasses?, Atmos. Chem. Phys., 8, 5221-5244, doi: 10.5194/acp-8-5221-2008, 2008.

726

727

728

729

730

731

732

733

734

735

736

737

738

739

740

741

742

745

746

747

748

749

750

751 **Table 1**. Summary of intensity ratio I_{SERS}/I_{NR} at peak bands of 937, 970, 1039 and 2930 cm^{-1}

752 for the AS, AS/SA and AS/sucrose particles and ambient PM. All Raman experiments were

753 conducted at ambient temperature and 60% RH.

Sample	Particle size [μm]	Particle phase	Intensity ratio			
			$\delta\,(OH{\cdots}O)$ ~937 cm^{-1}	$v\,(SO_4^{2-})$ ~970 cm^{-1}	$v\,(NO_3^-)$ ~1039 cm^{-1}	$v\,(C\text{-}H)$ ~2930 cm^{-1}
AS	31.6	Solid	NA	~ 1*	NA	NA
AS/SA	24.7	Solid	3.7	3.3	NA	2.6
	23.3		NA	12.4	NA	1.6
AS/sucrose	14.0		NA	14.8	NA	1.7
	4.0		NA	51.9	NA	6.9
	1.4	Aqueous	NA	162.0	NA	21.6
Ambient PM	<0.15	Solid	NA	1.9	1.6	NA

*No enhancement was observed at a band of $v\,(SO_4^{2-})$

754

755

756

757

758

759

760

761

762

763

764

765

766

767

768

769

Table 2. Peak position and full width at half maximum (FWHM) at the $v(SO_4^{2-})$ mode

Sample	Normal Raman		SERS	
	Sulfate peak [cm^{-1}]	FWHM [cm^{-1}]	Sulfate peak [cm^{-1}]	FWHM [cm^{-1}]
AS	977	7.9	977	7.5
AS/SA	977	7.4	965	20.0
AS/sucrose	980	13.5	967	16.9
Ambient PM	977	7.6	963	26.0

771

772

773

774

775

776

777

778

779

780

781

782

783

784

785

786

787

788

789

790

791
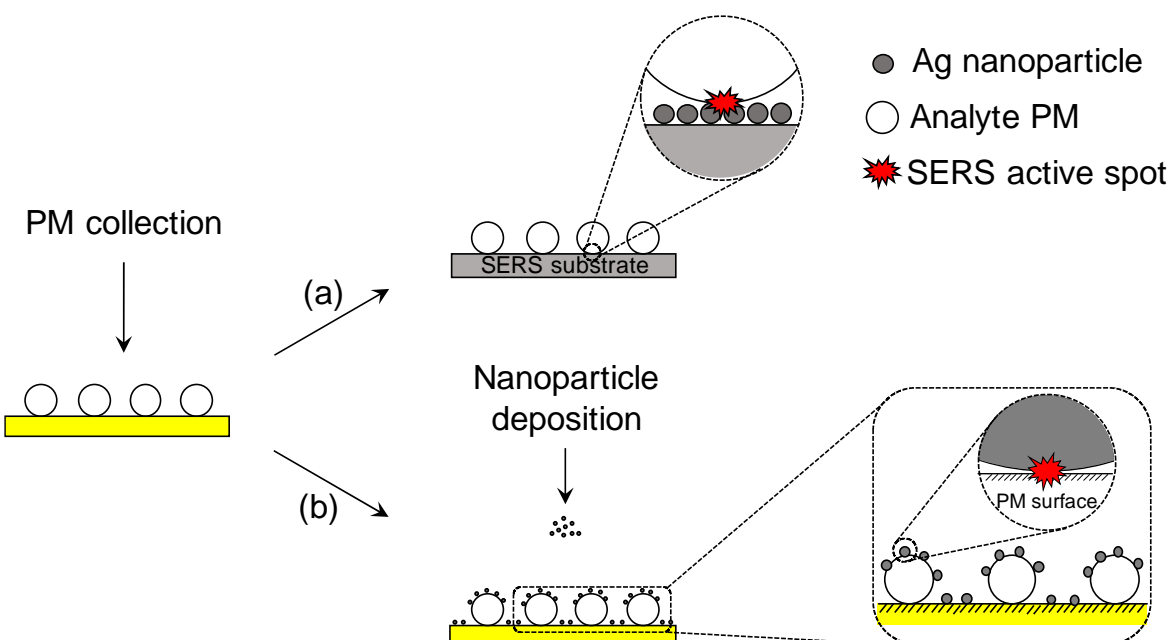
Figure 1. Schematic illustration of (a) a conventional SERS substrate approach and (b) the

proposed ES-SERS approach.

795

796

797

798

799

800

801

802

803

804

805

806

Carrier gas

Spray nozzle

Insulator

External electric field

Syringe pump

DMA

CPC

HV1

A

Substrate

HV2
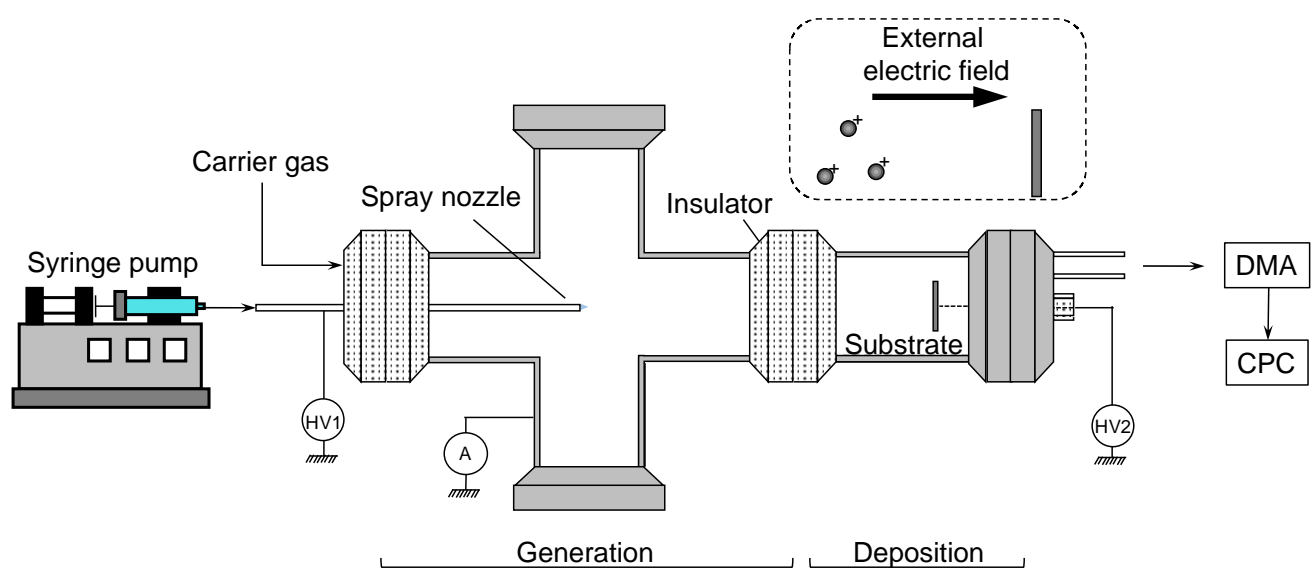
Generation

Deposition

Figure 2. Schematic illustration of the electrospray system consisting of a generation and a deposition chamber.

810

811

812

813

814

815

816

817

818

819

820

821

822

823

824

825
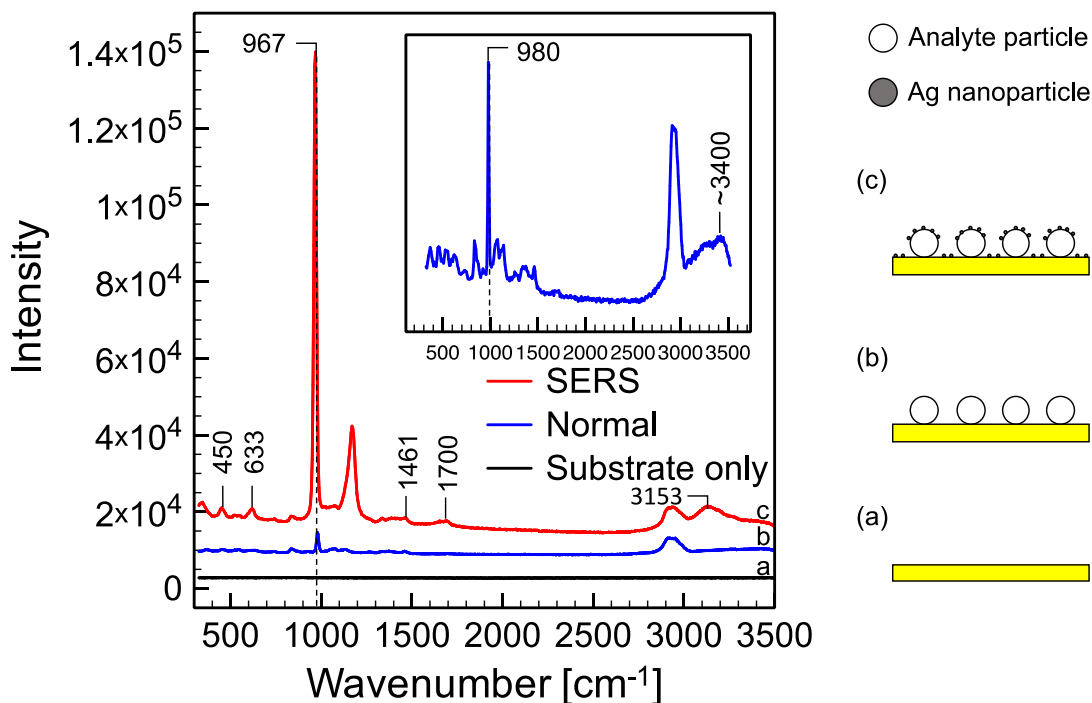
Figure 3. Normal Raman spectrum of substrate (black, a) and the AS/sucrose particles (blue,

b) and SERS spectrum of the AS/sucrose particles (red, c). The inset provides a magnified

view of the normal Raman spectrum for comparison. The particle sizes are 23.3 and 43.7 μm

for normal Raman and SERS experiments, respectively. Schematics represent (a) substrate

only, (b) analyte particles on substrate, and (c) analyte particles with Ag nanoparticles

deposited on a substrate.

832

833

834

835

836

837

838
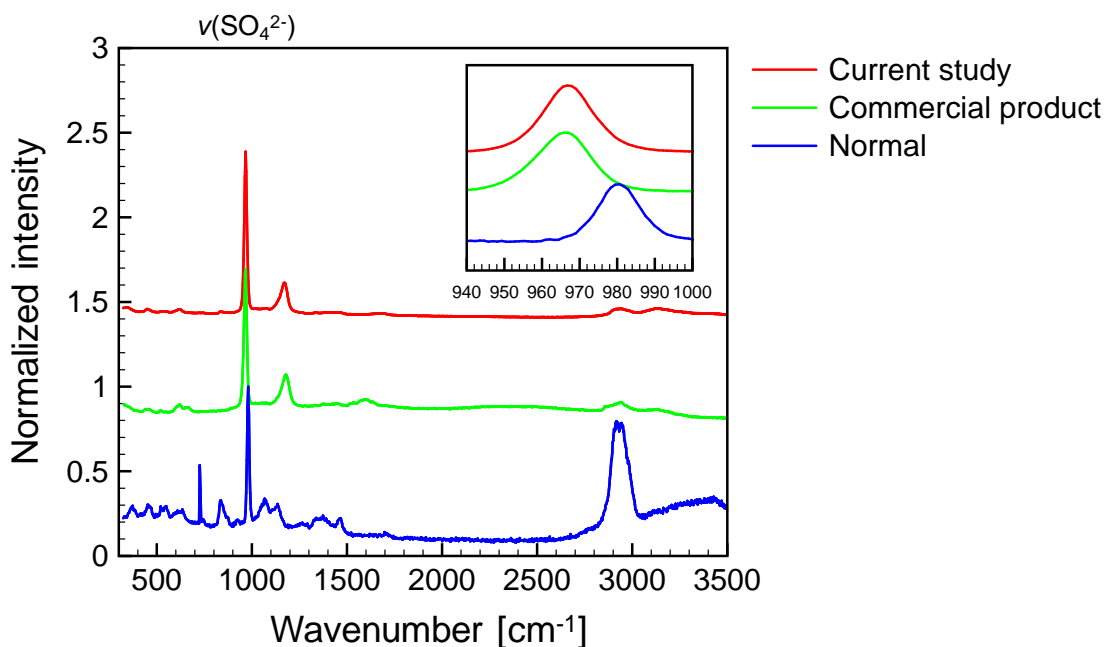
Figure 4. Normal (blue) and enhanced (green, commercial product; red, current SERS)

Raman spectra of the AS/sucrose particles. Inset frame is an enlarge view of spectra at 940-

1000 cm^{-1}.

842

843

844

845

846

847

848

849
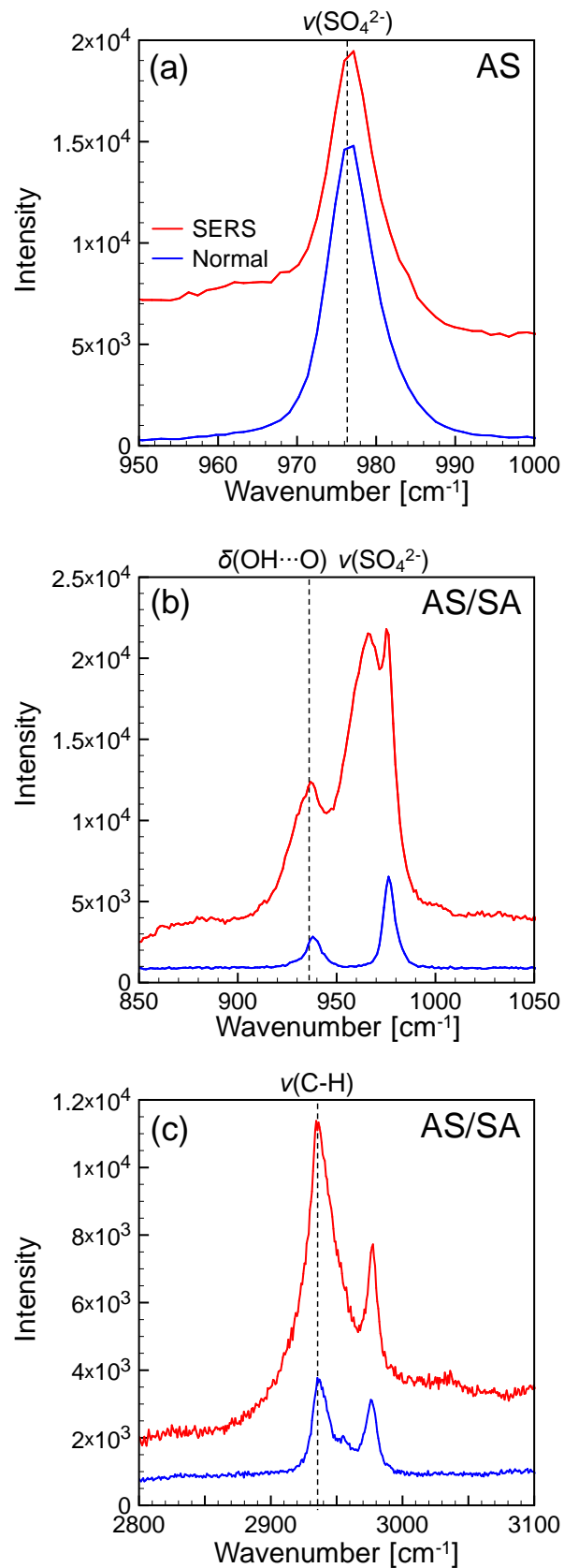
Figure 5. Normal and SERS spectra for (a) AS and (b) AS/SA particles at $v(SO_4^{2-})$ and (c)

v(C-H) (only applicable to the AS/SA particles) modes.

852

853

854

855

856

857

858
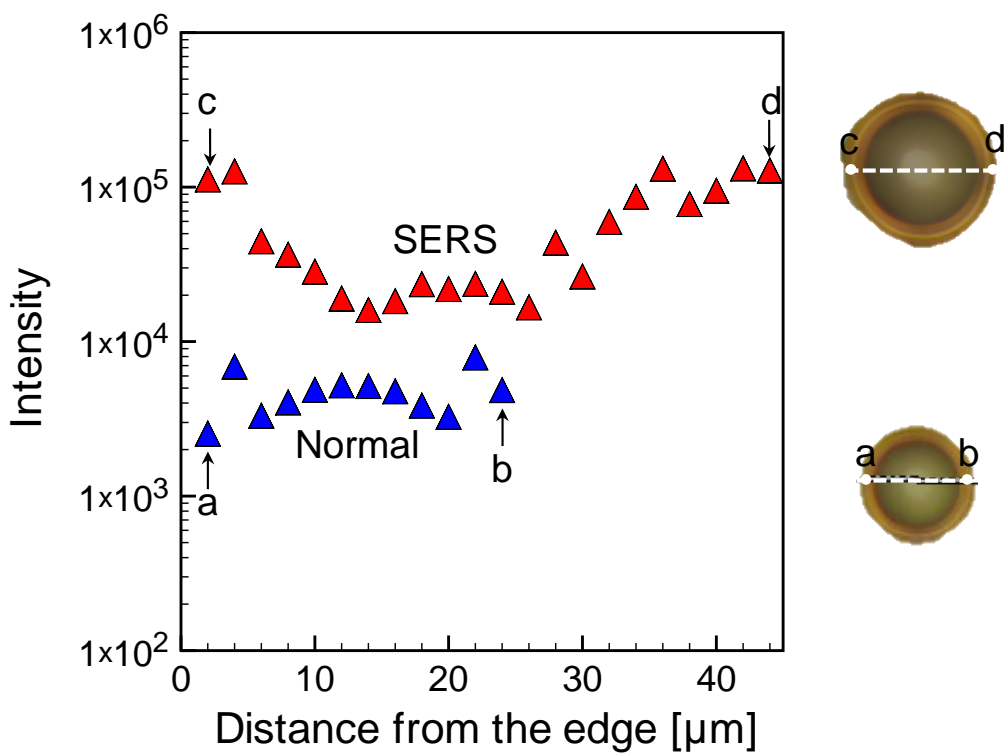
Figure 6. Raman intensity as a function of distance from edge to edge of the AS/sucrose

particles: point a to b for normal Raman (blue) and point c to d for SERS (red)

measurements. Optical images of corresponding particles were also shown.

862
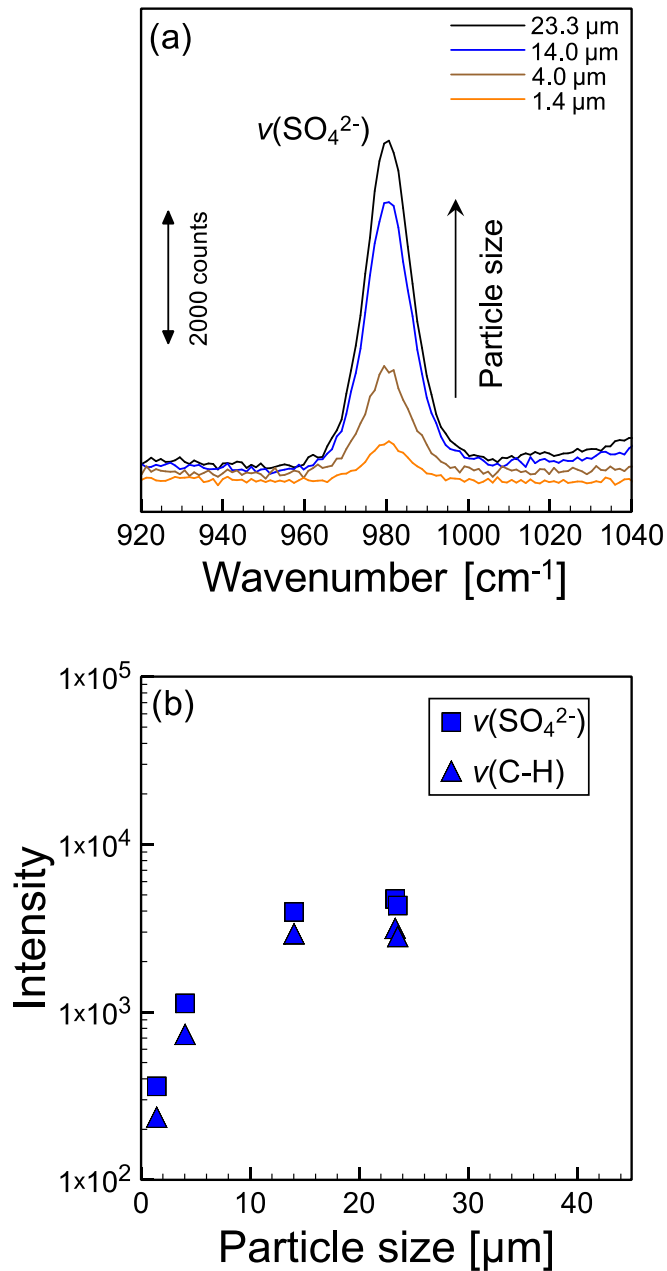
Figure 7. (a) Normal Raman spectra of the AS/sucrose particles as a function of particle size

in the lower energy region (920 ~ 1040 cm^{-1}). The peak band is assigned to the $v(SO_4^{2-})$

mode. (b) Raman intensity as a function of particle size for the $v(SO_4^{2-})$ and $v(C-H)$ modes.

866

867
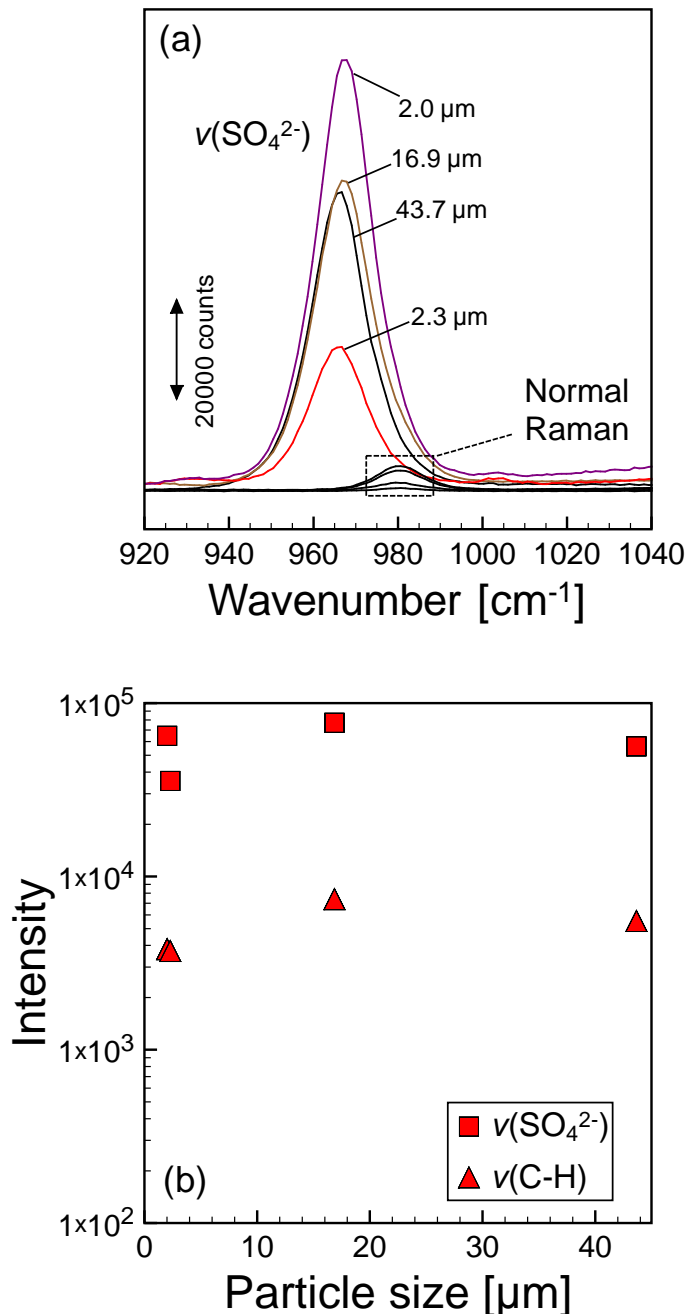
868

869 **Figure 8**. (a) Enhanced Raman spectra of the AS/sucrose particles as a function of particle

870 size in the lower energy region (920 ~ 1040 cm^{-1}). The peak band is assigned to the $v(SO_4^{2-})$

871 mode. The normal Raman spectra are also shown for comparison. (b) Raman intensity as a

872 function of particle size for the $v(SO_4^{2-})$ and $v(C\text{-}H)$ modes.

873

874
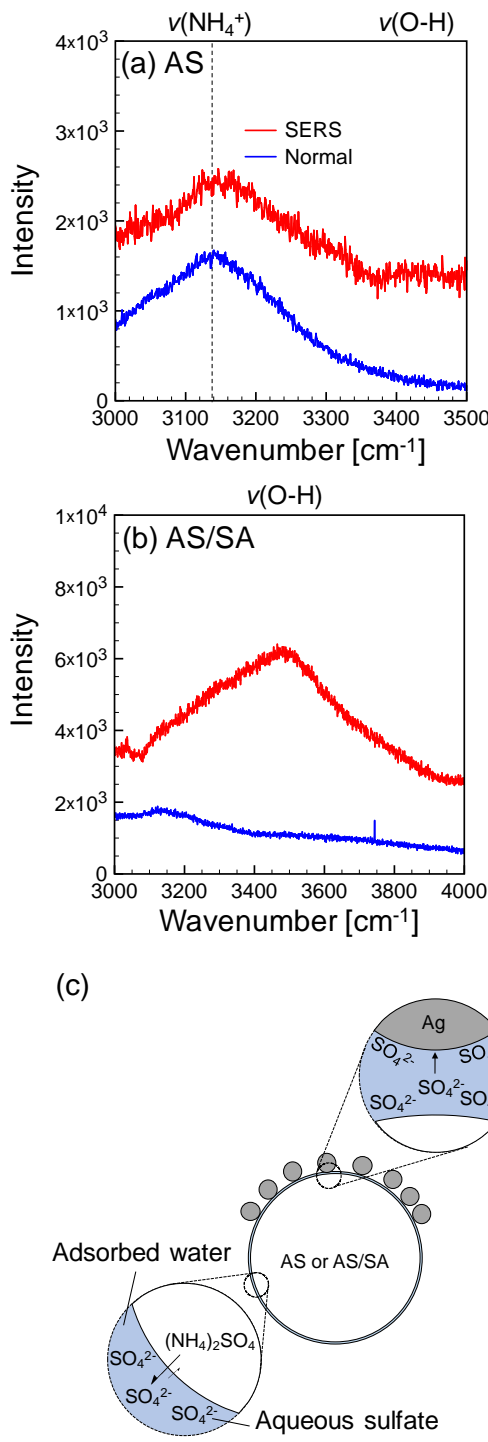
Figure 9. Normal (blue) and enhanced (red) Raman spectra of (a) AS and (b) AS/SA

particles at 3000 ~ 4000 cm^{-1}. The sizes of the AS particles are 31.6 and 30.3 µm for normal

Raman and SERS experiments, respectively. The sizes of the AS/SA particles are 24.7 and

25.5 µm for normal Raman and SERS experiments, respectively. (c) Schematic

representation (not to scale) of a possible role of surface-adsorbed water in facilitating

880 dissolution of aqueous sulfate anions that are subsequently chemisorbed on the surface of an

881 Ag nanoparticle.

882

883

884

885

886

887
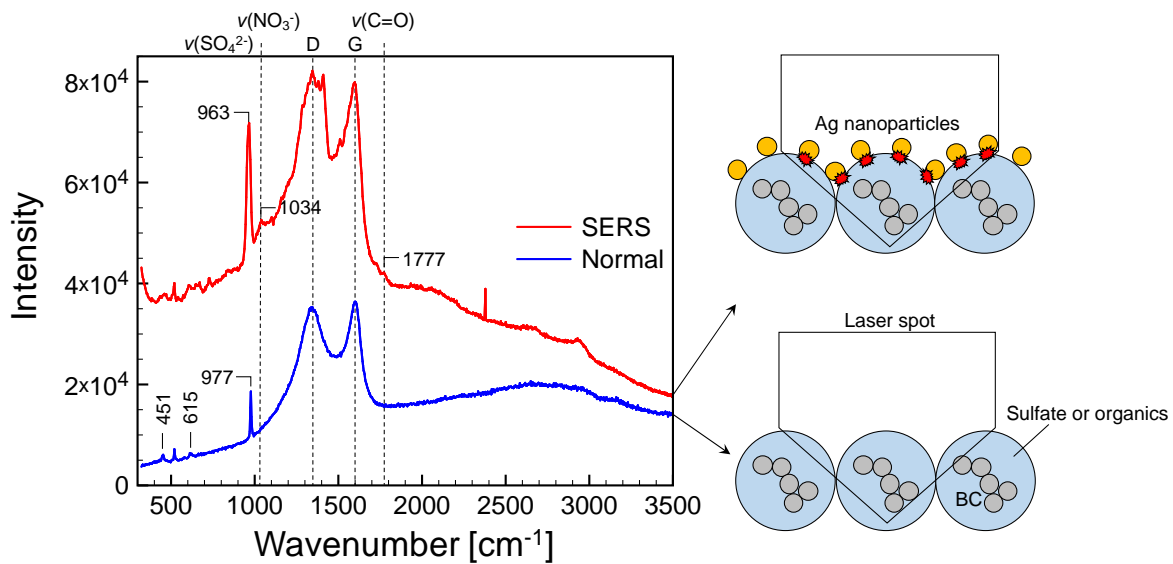
888

889 **Figure 10**. Normal (blue) and enhanced (red) Raman spectra of ambient PM. The particle size

890 is between 0.05 and 0.15 µm. Sulfate peaks at 451, 615 and 977 cm^{-1}, and D and G bands at

891 1341 and 1598 cm^{-1}, respectively, were observed. Enhanced spectra further showed peaks at

892 1039 (nitrate) and 1777 (carbonyl group, indicative of organic components) cm^{-1}. The

893 illustrations (not to scale) present experimental configurations for normal Raman and SERS

894 measurements. The normal spectrum includes the bulk chemical compositions of BC and

895 sulfate and the enhanced one includes the bulk compositions as well as the surface

896 compositions (i.e. sulfate and organics).

897